Dyes and Pigments 235 (2025) 112651

Contents lists available at ScienceDirect

Dyes and Pigments

journal homepage: www.elsevier.com/locate/dyepig

Outdoor durability of nano-sized silica-based chromatic reintegrations. Influence of exposure conditions and pigment composition

Daniel Jiménez-Desmond [a,*], José Santiago Pozo-Antonio [a], Anna Arizzi [b]

[a] CINTECX, GESSMin Group, Dpt. of Natural Resources and Environmental Engineering, School of Mining and Energy Engineering, University of Vigo, 36310, Vigo, Spain
[b] Dpt. of Mineralogy and Petrology, Faculty of Science, University of Granada, 18071, Granada, Spain

ARTICLE INFO

Keywords:
Binder
Inpainting
Environment
Outdoor exposure
Impurities
Painting conservation

ABSTRACT

Outdoor exposed wall paintings are highly vulnerable to decay from environmental factors such as solar radiation, humidity, and soluble salts. These factors can also affect the chromatic reintegrations in wall paintings. However, little research has been conducted on their durability. Therefore, a novel approach has been carried out by exploring the use of an aqueous colloidal dispersion of nano-sized silica as a binder in chromatic reintegrations under different environments. Thus, the binder was mixed with pigments (silicate-, oxide- and sulphide-based ones) to evaluate the influence of their chemical nature on the durability. Also, the paint mock-ups were exposed for one year to outdoor *Csb*- and *Dsa*-type environments (Köppen-Geiger climate classification system), in which moisture, temperature, rainfall and proximity to the sea differ considerably. Colour and gloss were measured before and after exposure. The paint samples were characterized using X-ray diffraction, Fourier transform infrared spectroscopy, Raman spectroscopy, and optical and scanning electron microscopies. After exposure, colour stability was highly influenced by the chemical nature of the pigments. A calcium-rich layer developed on all the mock-ups, together with other deposits, whose extent was highly influenced by the exposure conditions. Oxide-based pigments provided the best results, followed by the blue silicate-based ones. In contrast, sulphide-based and green earth-based pigments suffered substantial paint loss and colour changes. The different performance of the paintings was due to the affinity of the pigments with the binder and their predisposition to form bonds with hydroxyl (–OH), silanol (Si–OH) and siloxane (Si–O–Si) groups.

1. Introduction and research aim

Considerable research has been conducted in recent decades into the effects of atmospheric pollution, humidity and solar radiation on architectural heritage. The walls of historic buildings are often covered with a protective layer of rendering mortar that sometimes has an aesthetic function [1,2]. This is what happens with wall paintings. Even though some are carefully preserved in museums under stable conditions, most remain *in situ*, inseparable from the building in which they were placed. Those preserved *in situ*, and in particular those that are partially or completely exposed to the elements, are more vulnerable to deterioration due to the action of and/or fluctuations in different environmental agents (i.e. temperature, humidity, solar radiation, soluble salts, etc.) [3–5].

In general terms, when studying the state of conservation of outdoor-exposed wall paintings, moisture always appears as the main agent of decay [3,4]. This can cause various different alterations such as the detachment and consequent loss of the painted surface, forming what are known as 'lacunae' [4–6]. When this happens, professional restorers carry out a chromatic reintegration, also referred to as inpainting. The main goal is to replace the missing paint so as to allow the viewer to fully appreciate the artwork, with no interference from the lacunae or from the chromatic reintegration itself. The most widely used inpainting procedures reported in the literature are water-based (pigments generally dispersed in gum Arabic) and/or varnish-based (pigments dispersed in natural and synthetic resins) [4,7], although they only appear to be effective in indoor settings where the environmental conditions can be controlled [5,8]. For this reason, it is crucial to find an inpainting technique that can withstand the environmental fluctuations to which outdoor wall paintings are exposed [8].

Knowledge of the painting techniques (e.g., fresco, tempera, oil, acrylic, etc.) is also of great importance when it comes to developing strategies and specific measures for the conservation and restoration of wall paintings. The materials that make up historical wall paintings

* Corresponding author.
E-mail address: danieljose.jimenez@uvigo.es (D. Jiménez-Desmond).

https://doi.org/10.1016/j.dyepig.2025.112651
Received 6 November 2024; Received in revised form 13 January 2025; Accepted 14 January 2025
Available online 15 January 2025
0143-7208/© 2025 The Authors. Published by Elsevier Ltd. This is an open access article under the CC BY license (http://creativecommons.org/licenses/by/4.0/).

(mortar, pigment(s) and binder) behave differently with respect to the different decay agents. For instance, a fresco wall painting (which typically involves a pigment mixed with water that is fixed to the surface by carbonation of the lime mortar) will behave differently to a tempera (i.e. a pigment mixed with an organic binder such as egg yolk or rabbit glue) given that the nature of the binder and its affinity with the pigment (s) also vary. The materials used in conservation and restoration work must also be properly selected as even the most durable materials undergo a natural, progressive, irreversible process of degradation [9]. Unsuitable materials can damage the original painting, and it is therefore important to carefully select the right materials to guarantee optimum performance in terms of compatibility, durability and reversibility [8,10]. These three requirements are considered as ethical pillars in conservation and restoration [11].

If we consider an outdoor exposed wall painting, thus more vulnerable to deterioration, it is essential for the restorer to use a strong, resistant binder for inpainting. It is paramount that the selected binder ensures the natural breathability of the wall i.e. by creating a layer that allows the exchange of moisture between the wall and the environment. Despite this, research on the behaviour of materials used in outdoor exposed chromatic reintegrations is limited, particularly regarding their compatibility with the historical artwork and their long-term durability [8]. In this regard, the use of silicates as binders for wall paintings, a technique known as 'mineral painting' or 'stereochromy painting', was developed at the end of the 19th century. The aim was to find a painting technique that could withstand the inclement weather of Central Europe [12]. Nowadays, a range of silicate-based materials are available on the market as binders (sodium silicate, potassium silicate, alkoxysilanes, etc.). Previous research on one of these, the aqueous colloidal solution of nano-sized silica particles (10–20 nm), with formula $SiO_2{\cdot}nH_2O$, has demonstrated its potential as a binder for inpainting [13]. Silanol groups (Si–OH) form on the surface of the nano-silica particles (hydrogel) due to a condensation process [14,15]. After the water evaporates, the silica nanoparticles aggregate forming siloxane bonds (Si–O–Si), in which the hydrogel yields xerogel, thus forming a silica matrix [14–16], which could increase the capacity of the paint to withstand severe weather conditions [5].

Considering conservation and restoration ethical requirements [11], it is essential that the colour and texture of the chromatic reintegration match those of the original painting [11,17]. In a previous study [13], the visual and physical compatibility between nano-sized silica-based paint mock-ups (i.e. chromatic reintegration) and fresco paint mock-ups (i.e. historical painting) was evaluated. We must bear in mind the novelty of this procedure as this product has never been scientifically evaluated so far as binder for chromatic reintegration, as opposed to its use as nano-consolidant [18–22]. Overall, the nano-sized silica aqueous dispersion seemed to be a compatible binder for inpainting depending on the nature of the pigment used, thus complying with the first ethical requirement (i.e. compatibility among materials and between the historical painting and the chromatic reintegration itself). For instance, silicate-based pigments showed good affinity with the nano-silica binder in terms of the dispersion of the pigment within the binder and the adhesion of the chromatic reintegration to the mortar substrate [13]. Nevertheless, the encouraging results obtained by Ref. [13] regarding the compatibility of this novel inpainting technique is yet to be evaluated in terms of durability and reversibility.

With this in mind, the present study aim is to evaluate the durability (second ethical requirement [11]) of these chromatic reintegrations exposed to outdoor conditions, so as to validate its overall suitability as a potential binder for outdoor-exposed wall paintings. As pigments behave differently when exposed to decay agents [23], their chemical nature was also considered. Therefore, 8 pigments (4 silicates, 2 oxides and 2 sulphides) were applied *a fresco* and as a nano silica-based chromatic reintegration and subjected to natural outdoor aging for one year. The final aim was to evaluate i) the influence of the environment and ii) the influence of the chemical nature of the pigment on the durability of the reintegration. To achieve the first aim, two cities with completely different exposure conditions were selected. On the one hand, Vigo (NW Spain), with a humid environment and moderate temperatures, low pollution and marine influence. And on the other, Granada (SE Spain), with a dry environment and strong daily and seasonal temperature variations and high pollution. Although it is not influenced by the sea, it is affected by its proximity to Africa, as manifested in particulate matter from the Sahara Desert. In short, the exposure conditions (Vigo or Granada cities in the NW and SE of Iberian Peninsula respectively) and the chemical nature of the pigment (silicate-, oxide-, sulphur-based) have been considered here as crucial factors for the durability behaviour of the paint.

2. Materials and methods

2.1. Materials and mock-up preparation

A total of 8 pigments supplied by Kremer Pigments GmbH & Co. KG (Aichstetten, Germany) were selected for this study. They were grouped according to their chemical composition (silicates, oxides, sulphides) and manufacturing process (natural or synthetic). Egyptian blue (EG-B), lapis lazuli (LA-B), ultramarine blue (UL-B) and green earth (GE-G) (Fig. 1a) were chosen as silicates; mars red (MAR-R) and chromium green (CHR-G) as oxides (Fig. 1b); and cinnabar (CIN-R) and vermilion (VER-R) as sulphides (Fig. 1c). The presence of impurities in the silicate-based pigments, identified in previous research by Ref. [13], was also considered. For instance, the presence of phyllosilicates, such as muscovite ($KAl_2(AlSi_3O_{10})(OH)_2$), montmorillonite ($(Na,Ca)_{0,3}(Al,Mg)_2Si_4O_{10}(OH)_2 \cdot nH_2O$) or kaolinite ($Al_2Si_2O_5(OH)_4$)), must be taken into account when evaluating the durability of the paint, as some of them can swell up in the presence of moisture, so influencing the paint's long-term behaviour. As for oxide- and sulphide-based pigments, no impurities were identified by X-ray diffraction.

An aqueous colloidal dispersion of SiO_2 nanoparticles (around 10–20 nm), stabilized with sodium hydroxide (NaOH <0.5), commercialised as Nano Estel® by CTS S.L. (Madrid, Spain) [24], was used as a binder in the chromatic reintegrations. Paint mock-ups were also prepared following traditional recipes, as described in Ref. [13]. Pigments were applied on a lime-based mortar *a fresco* (hereinafter referred to as F, the lower part of the mock-ups in Fig. 1a–c) and mixed with nano-sized silica as a binder (hereinafter SB, the top part of the mock-ups in Fig. 1a–c). The complete physical, chemical and mineralogical characterization of the materials (pigments, binder, lime and aggregates) and the paint mock-ups is described in Ref. [13].

2.2. Natural outdoor exposure

Samples were positioned at an angle of 80° for a period of one year (July 2022 until July 2023) in two Spanish cities (Fig. 1d). One batch of samples was placed on the roof of a private house (42°13′58″N, 8°13′21″W) in the centre of Vigo (population 295,000), a city in the Galicia region of northwest Spain. Vigo is a major Atlantic port city with extensive industrial, commercial, fishing and shipbuilding activities. The samples were located 100 m away from the Vigo Ria estuary and from the canneries area. According to the Köppen-Geiger climate classification system, Vigo has a *Csb*-climate, in other words a 'warm-summer Mediterranean climate' with rainy winters and warm (rather than hot) summers. The other batch of samples was placed on the roof of the Faculty of Science (37°10′48″N, 3°36′33″W) of the University of Granada (population 230,000). Granada is a non-industrialized city in the region of Andalusia (SE Spain), situated at 680 m above sea level, about 50 km away from the Mediterranean coast and 200 km from the north coast of Africa. Granada has a peculiar situation: although it falls within the *Csa*-climate region with a 'hot-summer Mediterranean climate', its geographical location in a natural basin, surrounded by mountains with altitudes up to 3500 m gives it a *Dsa*-climate classification, i.e. a

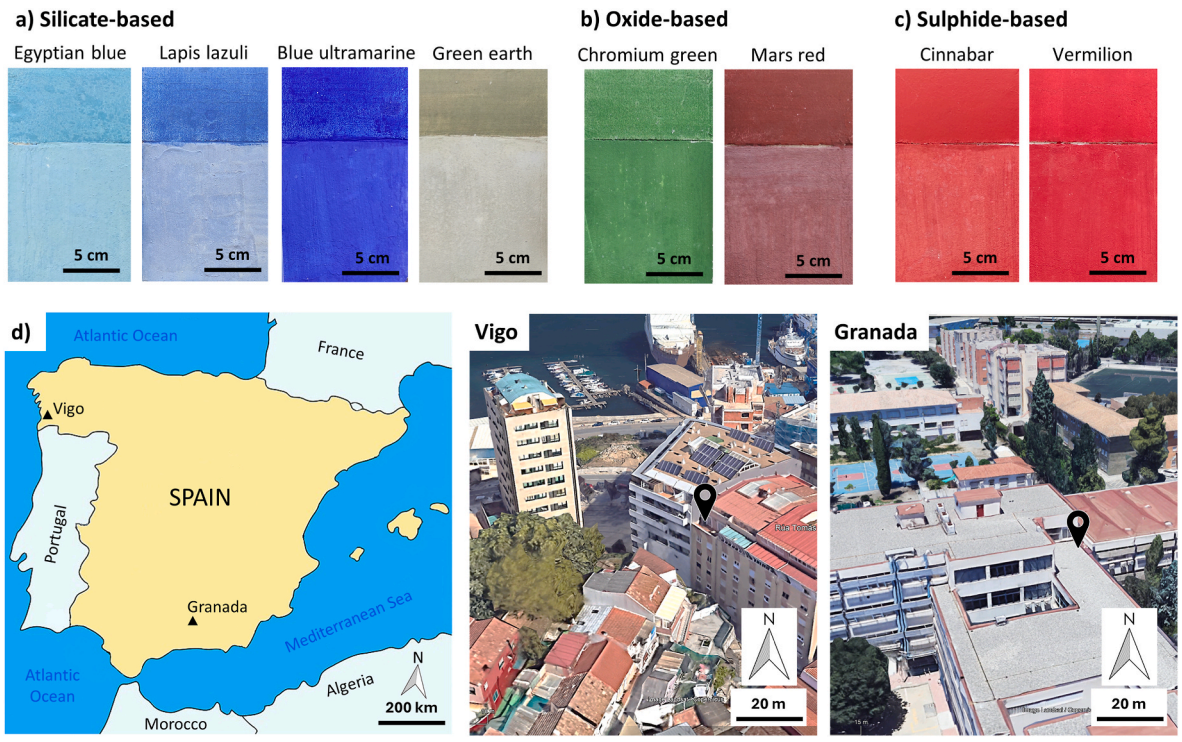


Fig. 1. a-c) Fresco (lower part) and nano-silica-based chromatic reintegration (top part) mock-ups before natural exposure. d) Map of Spain with the location of the cities of Vigo and Granada marked with black triangles, and aerial photographs showing the location of the paint mock-ups in each city.

continental climate with dry hot summers, cold winters, and high day/night temperature variability.

Table 1 presents a specific characterization of the environmental conditions at the two exposure sites with data on temperature, relative humidity, rainfall and air quality (SO_2, NO_2, PM_{10} and $PM_{2.5}$). The data was obtained from the Regional Government of Galicia and the University of Granada (accessed June 2024); therefore, accuracy of the data is guaranteed. On the one hand, in Vigo, data was obtained from a meteorological station located in the port (42°14′28″N, -8°43′31″W, 7 m altitude). Temperature and relative humidity results were obtained with a HMP155 Vaisala sensor (Vantaa, Finland); rainfall was measured with a 15189 LAMBRECHT meteo GmbH precipitation sensor (Göttingen, Germany) and an OTT HydroMet Parsivel^2 laser disdrometer (Kempten, Germany); finally, air quality was measured with a CR1000 Campbell measurement and control datalogger (Loughborough, United Kingdom). On the other hand, in Granada, the station was located in the Albaicín quarter (37°10′48″N, 3°35′26″W, 730 m altitude). Results were registered with a Davis Instruments Vantage Vue Professional Weather Station (Valencia, Spain). The accuracy, resolution and standards used for each equipment are specified by the suppliers.

2.3. Analytical techniques

The paint mock-ups were characterized before and after exposure to both environments with the following analytical techniques.

The texture and appearance of the surface of the mock-ups were studied with a Nikon SMZ 1000 microscope. Cross-sections were studied under Polarized-Light Microscopy (PLM), in both plane-polarised (PPL) and cross-polarised (XPL) light modes. For this, the specimens were embedded in epoxy resin (EpoThin 2 Epoxy Resin and EpoThin 2 Epoxy Hardener) and then cut and polished to a mirror shine.

The colour of the paint mock-ups was characterized using CIELAB and CIELCH colour spaces [25,26], measuring L* (lightness), a* and b* (colour coordinates) and C^*_{ab} (chroma) values using a Minolta CM-700d spectrophotometer. These parameters were measured every 50 days for 1 year. L* varies from 0 (black) to 100 (white). The other two parameters are chromaticity coordinates: a^* goes from red to green (where $+a^*$ is red and $-a^*$ is green) and b^* from yellow to blue ($+b^*$ is yellow and $-b^*$ is blue). C^*_{ab} is calculated according to the following formula: $C^*_{ab}=(a^2+b^2)^{1/2}$. The measurements were made in specular component excluded (SCE) mode, for a spot diameter of 8 mm, using illuminant D65 at an observer angle of 10°. A total of fifteen measurements were made

Table 1
Seasonal meteorological and air quality data, including standard deviations, for Vigo and Granada during the period July 2022–July 2023: Summer (July–September 2022), Autumn (October–December 2022), Winter (January–March 2023) and Spring (April–June 2023). More details can be found in Table S1 (from Supplementary Data) where the data obtained per month is presented.

		Temperature (°C)	Relative humidity (%)	Rainfall (L/m^2)	SO_2 (μg/m^3)	NO_2 (μg/m^3)	PM_{10} (μg/m^3)	$PM_{2.5}$ (μg/m^3)
VIGO (*Csb*-type climate)	Summer	20.87 ± 1.25	77.67 ± 5.13	30.43 ± 42.97	1.00 ± 0.00	15.19 ± 5.45	27.88 ± 12.23	14.72 ± 4.05
	Autumn	15.83 ± 2.27	81.33 ± 0.58	297.53 ± 30.07	1.17 ± 0.28	21.55 ± 4.91	25.03 ± 1.71	16.63 ± 2.35
	Winter	12.40 ± 1.23	72.67 ± 7.51	106.87 ± 109.98	1.40 ± 0.30	25.70 ± 9.13	29.00 ± 5.34	17.78 ± 3.39
	Spring	18.13 ± 2.10	75.33 ± 5.51	79.43 ± 19.03	6.45 ± 3.20	13.67 ± 2.48	22.69 ± 0.57	12.53 ± 0.82
GRANADA (*Dsa*-type climate)	Summer	25.70 ± 3.36	42.67 ± 7.38	3.67 ± 3.81	9.50 ± 2.08	13.56 ± 0.63	31.05 ± 4.80	14.20 ± 1.12
	Autumn	14.50 ± 5.20	64.00 ± 14.73	51.73 ± 69.62	7.77 ± 1.26	25.66 ± 4.42	29.64 ± 17.40	10.28 ± 3.43
	Winter	9.47 ± 3.38	62.67 ± 9.61	11.67 ± 8.18	7.49 ± 1.63	21.65 ± 6.14	22.20 ± 4.93	8.13 ± 1.46
	Spring	19.40 ± 2.77	50.67 ± 9.29	45.93 ± 43.22	9.57 ± 0.68	17.09 ± 4.89	20.63 ± 5.40	7.44 ± 0.34

for each mock-up and their average values and standard deviations (STD) were computed. Over the course of one year, various colour parameters of the exposed mock-ups were measured 7 times (once every 50 days): ΔL*, Δa*, Δb* and ΔC^*_{ab} colour differences and the total colour change (ΔE^*_{ab}) [25,26]. The measurements were calculated in comparison with the initial colour of each mock-up.

The gloss of the mock-ups was measured with a Novo-Gloss Lite 20/60/85° glossmeter, with a reflection angle of 60°, according to the Spanish standard UNE-EN ISO 2813 [27]. Five measurements were taken per sample and their average value and standard deviation (STD) were calculated.

The mineralogical composition of the paint mock-ups was determined using micro X-ray diffraction (μXRD) according to the random-powder method. A BRUKER D8 DISCOVER diffractometer was used with a PILATUS3R 100K-A detector. Analyses were performed using Cu-Kα radiation (λ = 1,5406 Å), Ni filter, a voltage of 50 kV, and a current of 1 mA. The exploration range was 5°–75° 2θ and the goniometer speed was 0.02° 2θ s^{-1}. The mineral phases were identified using X'Pert HighScore software.

Further studies were made of the chromatic reintegration mock-ups (SB) that performed best and the fresco mock-ups (F) that underwent the greatest changes. Their molecular composition was obtained by Attenuated Transmittance Reflectance Fourier–Transform Infrared Spectroscopy (ATR-FTIR) using a Thermo Nicolet 6700 at a resolution of 2 cm^{-1} over 100 scans in the mid infrared spectral region (400–4000 cm^{-1}). For the CIN-R and VER-R paint mock-ups, FTIR spectra were also taken in the 50–400 cm^{-1} infrared spectral region, where IR bands characteristic of sulphides are present.

Chemical characterization of the paint layer of the mock-ups was carried out using a portable i-Raman Prime spectrometer BWS475-1064 manufactured by B&W TEK (Metrohm Group Company). The equipment operates at a wavelength of 1064 nm, with a resolution of <10 cm^{-1} and a nominal energy of 340 mW. It has an integration time of 0.2 ms–5 min, coupled with a High Sensitivity InGaAs Array detector. The parameters used in this study were: an integration time of 500 ms, laser power of 8 and an average time of 20.

The microtexture and elemental composition of all the paint mock-ups (F and SB) were studied using a JEOL JSM 6010LA scanning electron microscopy (SEM) with energy-dispersive X-ray spectroscopy (EDS) in both secondary (SE) and backscattered electron (BSE) detection modes. Observation conditions included a working distance of around 10 mm, an accelerating potential of 20 kV and a specimen current of ~60 mA. Samples were studied by observing the surface directly, and by studying the paint layer in cross-sections.

3. Results

3.1. Stereomicroscopy

Fig. 2 shows micrographs of the surface of all the fresco (F) and nano-silica-based chromatic reintegration (SB) mock-ups, before and after one year of natural exposure in Vigo (VI) and Granada (GR). The greatest visual changes were recorded in the paint mock-ups exposed in Granada, i.e. with a *Dsa*-type climate. Particles of different morphology and size, together with brownish deposits, were observed on the surface, especially in the F-based mock-ups, regardless of the pigment used. In addition, occasional whitish veils (e.g. Fig. 2f) were observed on the surface of all the paint mock-ups, although they were more evident in SB paints, and covered larger areas in those from Vigo (*Csb*-type climate). The chromatic reintegrations (SB) that showed serious alterations after one year of natural exposure, in both VI and GR, were green earth (GE-G, Fig. 2h), cinnabar (CIN-R, Fig. 2m and n) and vermilion (VER-R, Fig. 2o and p) paints. Indeed, on the mock-ups painted with these three pigments, the SB paint layer was missing to a greater or lesser extent, regardless of the environmental exposure conditions. The CIN-R and VER-R paints (F and SB) also underwent major colour changes, from greyish-brown to black, which were more pronounced in the Vigo mock-ups.

3.2. Colour spectrophotometry and gloss measurement

The colour difference(ΔE^*_{ab}) calculated after periodic monitoring (every 50 days) of the colour in all the paint mock-ups is shown in Fig. 3. The black-dashed line marks 3.5 CIELAB units. i.e. the value from which colour variations are visible to the naked eye [28]. Regardless of the colorimetric changes, ΔE^*_{ab} values became increasingly stable over the 350-day exposure period. In terms of exposure sites (VI or GR), no major differences were observed between the two sites except for LA-B-F (Fig. 3c) in Vigo, which underwent greater change. Conversely, for the case of sulphide-based F and SB paints (Fig. 3m–p) and GE-G-SB (Fig. 3h), the colour variation observed after the first 50 days of exposure was higher in Granada (ΔE^*_{ab} > 20 CIELAB units). However, the changes recorded after 350 days were similar in both locations, implying that colour variations were more gradual in Vigo. ΔE^*_{ab} values were also influenced by the chemical composition (silicates, oxides or sulphides). The oxide-based paints (Fig. 3i–l) underwent the lowest changes in colour (ΔE^*_{ab} < 5 CIELAB units), followed by the blue silicate-based paints (EG-B, LA-B and UL-B, Fig. 3a–f respectively) with an ΔE^*_{ab} of around 5 units. As for the green-silicate paints, the F paints generally had values of less than 5 CIELAB units (Fig. 3g). In the SB paints, by contrast, the ΔE^*_{ab} was over 30 CIELAB units (Fig. 3h). This was probably due to the loss of the paint layer, as seen in Fig. 2h. The paints that underwent the highest colour variations were F and SB sulphide-based paints (Fig. 3m–p), so confirming the high colour change observed by stereomicroscopy (Fig. 2m–p). Lastly, the origin of the pigment (natural or synthetic) did not seem to have a decisive influence: LA-B and UL-B showed similar results, as did CIN-R and VER-R (natural and synthetic respectively).

As for gloss, Fig. 4 shows the gloss values (G) before (reference) and after exposure. A general decrease in these values was detected in all the samples after 350 days of direct outdoor exposure regardless of the exposure conditions, the pigment or the painting technique. The only exception was GE-G-SB, where G values increased (Fig. 4b). Therefore, the SB-based samples that performed best (under naked eye observations, stereomicroscopy and colour spectrophotometry) after 1 year of natural exposure were EG-B, LA-B, UL-B, MAR-R and CHR-G.

3.3. Micro-X-ray diffraction (μXRD)

The mineralogical composition of all the SB samples was very similar before and after 350 days of natural outdoor exposure (Table 2). Minerals from the chlorite group (clinochlore, $(Mg,Fe^{2+})_5Al(Si_3Al)O_{10}(OH)_8$) were present in the UL-B paints at the end of the exposure period. These are usually associated with the hydrothermal reaction of kaolinite (used in the manufacture of this synthetic pigment) [29,30]. Gypsum ($CaSO_4{\cdot}2H_2O$) was also identified in some of the exposed samples, mainly in those from Vigo, regardless of the painting technique or pigment used. We also observed that none of the minerals related to green earth-based paints (mainly glauconite or celadonite, among other compounds) were present after outdoor exposure.

3.4. Attenuated total reflectance-fourier transform infrared spectroscopy (ATR-FTIR)

In order to evaluate possible binder-related chemical changes in the chromatic reintegrations (SB) after the natural aging test, a molecular characterization with FTIR was carried out before and after exposure. The characterization of the binder (NE), without pigment (Fig. 5a), showed bands at 3700-2800 (Si–OH stretching), 1645 (H–*O*–H) and 960 cm^{-1} (Si–OH stretching) related to silanol groups [31,32]. Bands were observed at 2958 and 2885 cm^{-1} associated with C–H stretching vibrations, generally from residual solvent (ethanol) or alkylamine chains

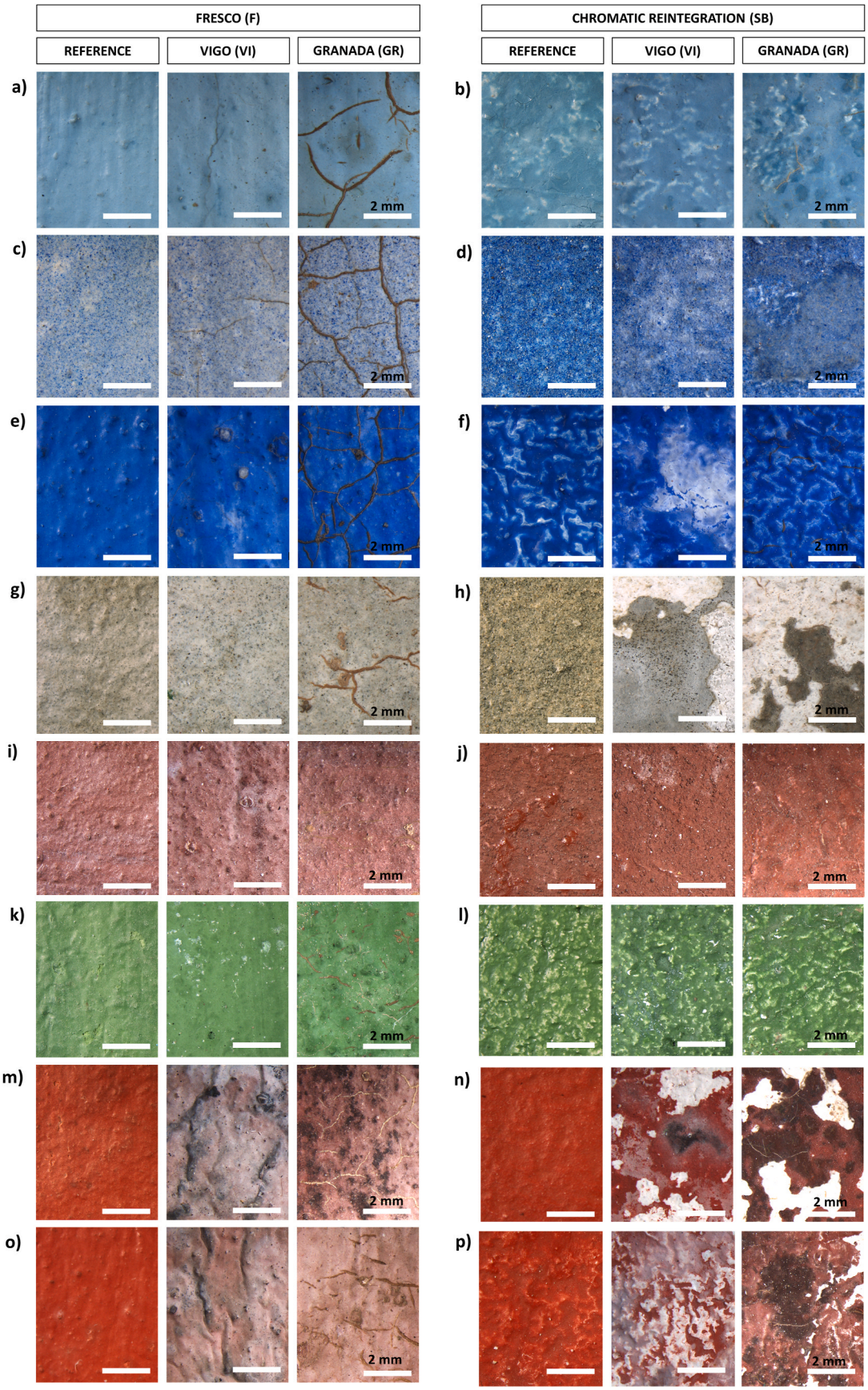


Fig. 2. Micrographs of the paint mock-ups (fresco-F and nano-silica-based-SB) before (Reference) and after one year of outdoor exposure in Vigo and Granada. Paint mock-ups with a-b) Egyptian blue; c-d) lapis lazuli); e-f) ultramarine blue; g-h) green earth; i-j) Mars red; k-l) chromium green; m-n) cinnabar; and o-p) vermilion.

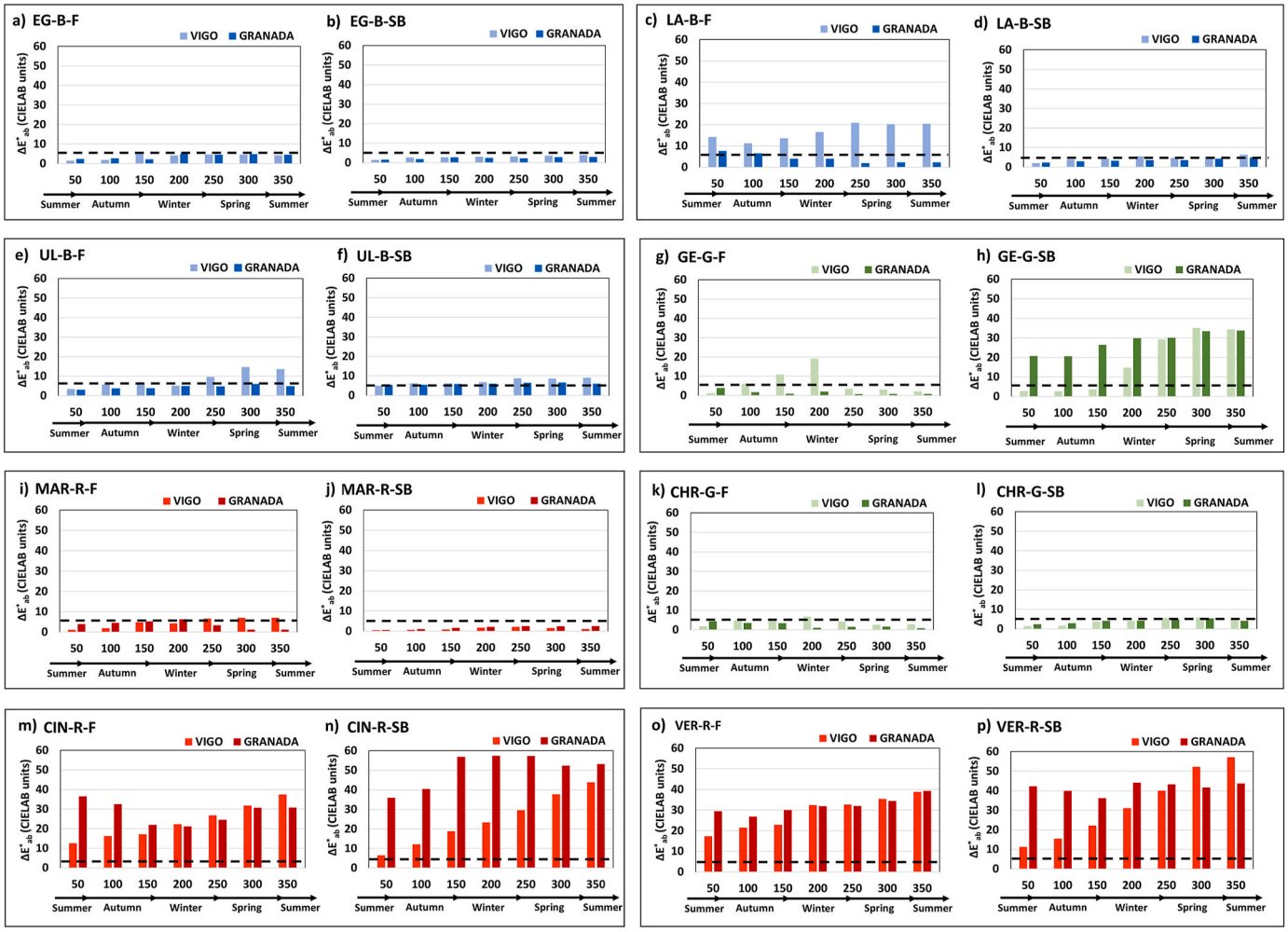


Fig. 3. ΔE^*_{ab} (CIELAB units) for the outdoor-exposed paint mock-ups in Vigo and Granada: a-b) Egyptian blue (EG-B); c-d) lapis lazuli (LA-b); e-f) ultramarine blue (UL-B); d-g) green earth (GE-G); i-j) mars red (MAR-R); k-l) chromium green (CHR-G); m-n) cinnabar (CIN-R); and o-p) vermilion (VER-R).

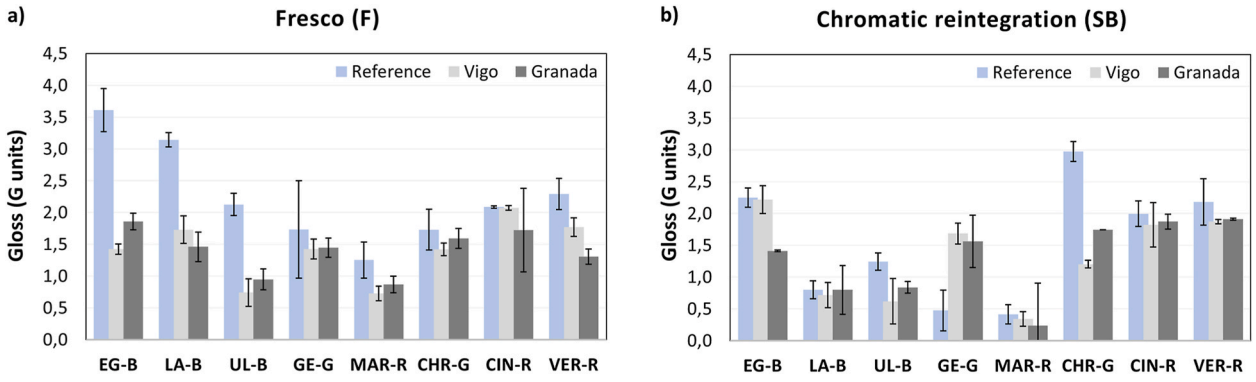


Fig. 4. Average gloss (G units) values for a) fresco (F) and b) nano-sized silica-based chromatic reintegration mock-ups (SB) with their standard deviations. Each figure contains gloss values for unpainted (FR), Egyptian blue (EG-B), lapis lazuli (LA-B), ultramarine blue (UL-B), Mars red (MAR-R), chromium green (CHR-G), cinnabar (CIN-R), vermilion (VER-R) and green earth (GE-G) mock-ups before (Reference) and after exposure in Vigo and Granada.

related to ammonia (NH_3) [31,32], indicating that water was not the only solvent. The presence of these weak bands ascribable to an alcohol or ammonia is not surprising as they are used in the synthesis process to obtain silica nanoparticles [33,34]. The bands present at ≈1080-1040, 790 and 445 cm^{-1} (Si–O) are related to the formation of a silica gel (SiO_2) [31,32].

In this phase, we only studied those SB paint mock-ups that performed well in the earlier tests involving naked eye, stereo-microscopy and colour spectrophotometry observation i.e. EG-B, LA-B, UL-B, MAR-R and CHR-G. As mentioned above, the paint layer in CIN-R, VER-R and GE-G SB mock-ups was missing after one year of exposure, indicating low affinity between the pigment and the nano estel (NE). In general terms, in all the mock-ups, regardless of the exposure conditions or the pigment, bands associated with calcium carbonate (marked with

Table 2
Mineralogical characterization by micro-X-ray diffraction (μXRD) of the mock-ups painted with Egyptian blue (EG-B), lapis lazuli (LA-B), ultramarine blue (UL-B), Mars red (MAR-R), chromium green (CHR-G), cinnabar (CIN-R), vermilion (VER-R) and green earth (GE-G). The mineral phases identified in both painting techniques (F and SB) before and after natural exposure in Vigo (VI) and Granada (GR) are shown.

Paints before exposure	Mineralogical characterization before exposure	Paints after exposure	Mineralogical characterization after exposure
EG-B-F	Calcite ($CaCO_3$), cuprorivaite ($CaCuSi_4O_{10}$)	EG-B-F-VI	Cuprorivaite ($CaCuSi_4O_{10}$), calcite ($CaCO_3$), gypsum ($CaSO_4{\cdot}2H_2O$)
		EG-B-F-GR	Cuprorivaite ($CaCuSi_4O_{10}$), calcite ($CaCO_3$), gypsum ($CaSO_4{\cdot}2H_2O$)
EG-B-SB	Calcite ($CaCO_3$), cuprorivaite ($CaCuSi_4O_{10}$)	EG-B-SB-VI	Cuprorivaite ($CaCuSi_4O_{10}$), calcite ($CaCO_3$), gypsum ($CaSO_4{\cdot}2H_2O$)
		EG-B-SB-GR	Cuprorivaite ($CaCuSi_4O_{10}$), calcite ($CaCO_3$), gypsum ($CaSO_4{\cdot}2H_2O$)
LA-B-F	Calcite ($CaCO_3$), lazurite ($Na_3Ca(Al_3Si_3O_{12})S$), diopside ($CaMgSi_2O_6$), pyrite (FeS_2), wollastonite ($CaSiO_3$)	LA-B-F-VI	Lazurite ($Na_3Ca(Al_3Si_3O_{12})S$), sodalite ($Na_8Al_6Si_6O_{24}Cl_2$), calcite ($CaCO_3$)
		LA-B-F-GR	Lazurite ($Na_3Ca(Al_3Si_3O_{12})S$), calcite ($CaCO_3$), gypsum ($CaSO_4{\cdot}2H_2O$)
LA-B-SB	Calcite ($CaCO_3$), lazurite ($Na_3Ca(Al_3Si_3O_{12})S$), sodalite ($Na_8Al_6Si_6O_{24}Cl_2$), diopside ($CaMgSi_2O_6$), pyrite (FeS_2), muscovite ($KAl_2Si_3AlO_{10}(OH)_2$)	LA-B-SB-VI	Lazurite ($Na_3Ca(Al_3Si_3O_{12})S$), sodalite ($Na_8Al_6Si_6O_{24}Cl_2$), calcite ($CaCO_3$), diopside ($CaMgSi_2O_6$), muscovite ($KAl_2Si_3AlO_{10}(OH)_2$)
		LA-B-SB-GR	Lazurite ($Na_3Ca(Al_3Si_3O_{12})S$), sodalite ($Na_8Al_6Si_6O_{24}Cl_2$), calcite ($CaCO_3$), diopside ($CaMgSi_2O_6$), muscovite ($KAl_2Si_3AlO_{10}(OH)_2$)
UL-B-F	Calcite ($CaCO_3$), lazurite ($Na_3Ca(Al_3Si_3O_{12})S$), sodalite ($Na_8Al_6Si_6O_{24}Cl_2$), nepheline (Na,K$(Al_4Si_4O_{16})$)	UL-B-F-VI	Lazurite ($Na_3Ca(Al_3Si_3O_{12})S$), calcite ($CaCO_3$), quartz (SiO_2), nosean ($Na_8Al_6Si_6O_{24}(SO_4)$), clinochlore ($(Mg,Fe^{2+})_5Al(Si_3Al)O_{10}(OH)_8$)
		UL-B-F-GR	Lazurite ($Na_3Ca(Al_3Si_3O_{12})S$), calcite ($CaCO_3$), nepheline (Na,K$(Al_4Si_4O_{16})$), clinochlore ($(Mg,Fe^{2+})_5Al(Si_3Al)O_{10}(OH)_8$)
UL-B-SB	Calcite ($CaCO_3$), lazurite ($Na_3Ca(Al_3Si_3O_{12})S$), portlandite ($Ca(OH)_2$), kaolinite ($Al_2Si_2O_5(OH)_4$)	UL-B-SB-VI	Lazurite ($Na_3Ca(Al_3Si_3O_{12})S$), calcite ($CaCO_3$), clinochlore ($(Mg,Fe^{2+})_5Al(Si_3Al)O_{10}(OH)_8$)
		UL-B-SB-GR	Lazurite ($Na_3Ca(Al_3Si_3O_{12})S$), calcite ($CaCO_3$), nepheline (Na,K$(Al_4Si_4O_{16})$), clinochlore ($(Mg,Fe^{2+})_5Al(Si_3Al)O_{10}(OH)_8$)
GE-G-F	Calcite ($CaCO_3$), glauconite ((K,Na)$(Fe^{3+},Al,Mg)_2(Si,Al)_4O_{10}(OH)_2$), celadonite (K(Mg,Fe)$Fe^{3+}Si_4O_{10}(OH)_2$)	GE-G-F-VI	Calcite ($CaCO_3$)
		GE-G-F-GR	Calcite ($CaCO_3$), gypsum ($CaSO_4{\cdot}2H_2O$), quartz (SiO_2)
GE-G-SB	Calcite ($CaCO_3$), glauconite ((K,Na)$(Fe^{3+},Al,Mg)_2(Si,Al)_4O_{10}(OH)_2$), celadonite (K(Mg,Fe)$Fe^{3+}Si_4O_{10}(OH)_2$), quartz ($SiO_2$), muscovite ($KAl_2Si_3AlO_{10}(OH)_2$)	GE-G-SB-VI	Calcite ($CaCO_3$)
		GE-G-SB-GR	Calcite ($CaCO_3$), quartz (SiO_2)
MAR-R-F	Calcite ($CaCO_3$), hematite (Fe_2O_3)	MAR-R-F-VI	Hematite (Fe_2O_3), calcite ($CaCO_3$)
		MAR-R-F-GR	Hematite (Fe_2O_3), calcite ($CaCO_3$), quartz (SiO_2)
MAR-R-SB	Calcite ($CaCO_3$), hematite (Fe_2O_3)	MAR-R-SB-VI	Hematite (Fe_2O_3), calcite ($CaCO_3$)
		MAR-R-SB-GR	Hematite (Fe_2O_3), calcite ($CaCO_3$)
CHR-G-F	Calcite ($CaCO_3$), eskolaite (Cr_2O_3)	CHR-G-F-VI	Eskolaite (Cr_2O_3), calcite ($CaCO_3$), gypsum ($CaSO_4{\cdot}2H_2O$)
		CHR-G-F-GR	Eskolaite (Cr_2O_3), calcite ($CaCO_3$)
CHR-G-SB	Calcite ($CaCO_3$), eskolaite (Cr_2O_3), quartz (SiO_2)	CHR-G-SB-VI	Eskolaite (Cr_2O_3), calcite ($CaCO_3$), gypsum ($CaSO_4{\cdot}2H_2O$)
		CHR-G-SB-GR	Eskolaite (Cr_2O_3), calcite ($CaCO_3$), quartz (SiO_2)
CIN-R-F	Calcite ($CaCO_3$), cinnabar (HgS)	CIN-R-F-VI	Cinnabar (HgS), calcite ($CaCO_3$), quartz (SiO_2), dolomite ($CaMg(CO_3)_2$)
		CIN-R-F-GR	Cinnabar (HgS), calcite ($CaCO_3$), quartz (SiO_2), dolomite ($CaMg(CO_3)_2$)
CIN-R-SB	Calcite ($CaCO_3$), cinnabar (HgS)	CIN-R-SB-VI	Cinnabar (HgS), calcite ($CaCO_3$), quartz (SiO_2), gypsum ($CaSO_4{\cdot}2H_2O$)
		CIN-R-SB-GR	Cinnabar (HgS), calcite ($CaCO_3$), quartz (SiO_2)
VER-R-F	Calcite ($CaCO_3$), cinnabar (HgS), portlandite ($Ca(OH)_2$)	VER-R-F-VI	Cinnabar (HgS), calcite ($CaCO_3$), gypsum ($CaSO_4{\cdot}2H_2O$)
		VER-R-F-GR	Cinnabar (HgS), calcite ($CaCO_3$), quartz (SiO_2), gypsum ($CaSO_4{\cdot}2H_2O$)
VER-R-SB	Calcite ($CaCO_3$), cinnabar (HgS), portlandite ($Ca(OH)_2$)	VER-R-SB-VI	Cinnabar (HgS), calcite ($CaCO_3$), quartz (SiO_2), gypsum ($CaSO_4{\cdot}2H_2O$)
		VER-R-SB-GR	Cinnabar (HgS), calcite ($CaCO_3$)

black arrows in Fig. 5g) appeared at 1795 cm^{-1} (C═O), ≈1400 cm^{-1} (CO_3^{2-} stretching), ≈870 cm^{-1} (CO_3^{2-} antisymmetrical bending) and ≈715 cm^{-1} (CO_3^{2-} symmetrical bending) [35,36], in line with the XRD results. However, in EG-B-SB, the bands assigned to $CaCO_3$ were more intense (marked with black arrows in Fig. 5c) in the Vigo (*Csb*-type climate) samples, than in those from Granada. Although a band at ≈3640 cm^{-1} (Ca–OH), related to portlandite-$Ca(OH)_2$- [37,38], was often present in the reference paint mock-ups (Fig. 5b and e), it was not present in any of the paints after exposure, indicating complete carbonation of the lime mortar after one year.

As for the NE binder, low intensity bands associated to silanol groups (Si–OH) were observed in all the paint mock-ups (EG-B, LA-B, UL-B, MAR-R, CHR-G), as marked with a red dashed line in Fig. 5. Bands associated with Si–O and the formation of silica gel (1065, 1045, 790 and 445 cm^{-1}) were occasionally present. In the case of EG-B-SB (Fig. 5b–d), these bands overlapped with those related with the raw pigment, cuprorivaite ($CaCuSi_4O_{10}$), at 1050 and 1005 cm^{-1} (Si–O antisymmetrical stretching), and 470 and 420 cm^{-1} (Si–O bond) [39]. However, in the other SB mock-ups, regardless of the exposure site or the pigment, the band at ≈790 cm^{-1} was less intense after exposure, forming a shoulder. The band at 445 cm^{-1} was always present, especially in MAR-R-SB (Fig. 5e–g). The bands at 1065 and 1045 cm^{-1} were

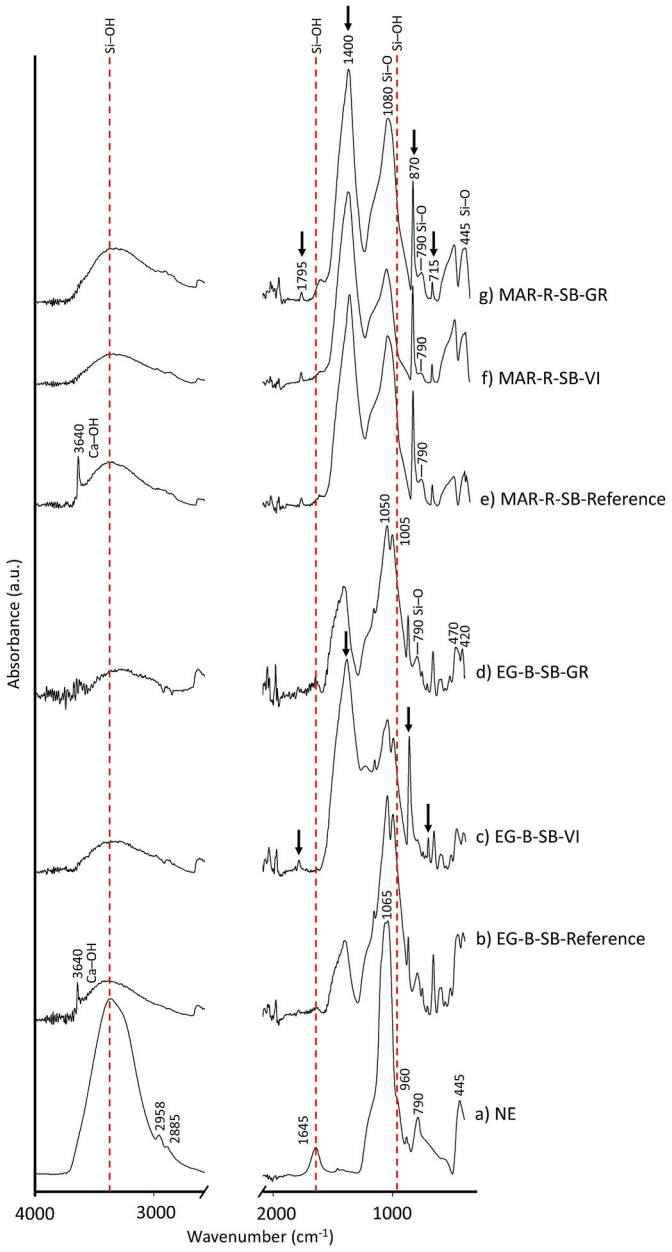


Fig. 5. ATR-FTIR spectra in the mid-IR (4000-600 cm-1) for: a) nano estel (NE) without pigment; b-d) EG-B-SB reference paint mock-ups and mock-ups exposed in Vigo (VI) and Granada (GR); and e-g) MAR-R-SB reference paint mock-ups and mock-ups exposed in Vigo (VI) and Granada (GR). The black arrows indicate the presence of characteristic bands associated with calcium carbonate.

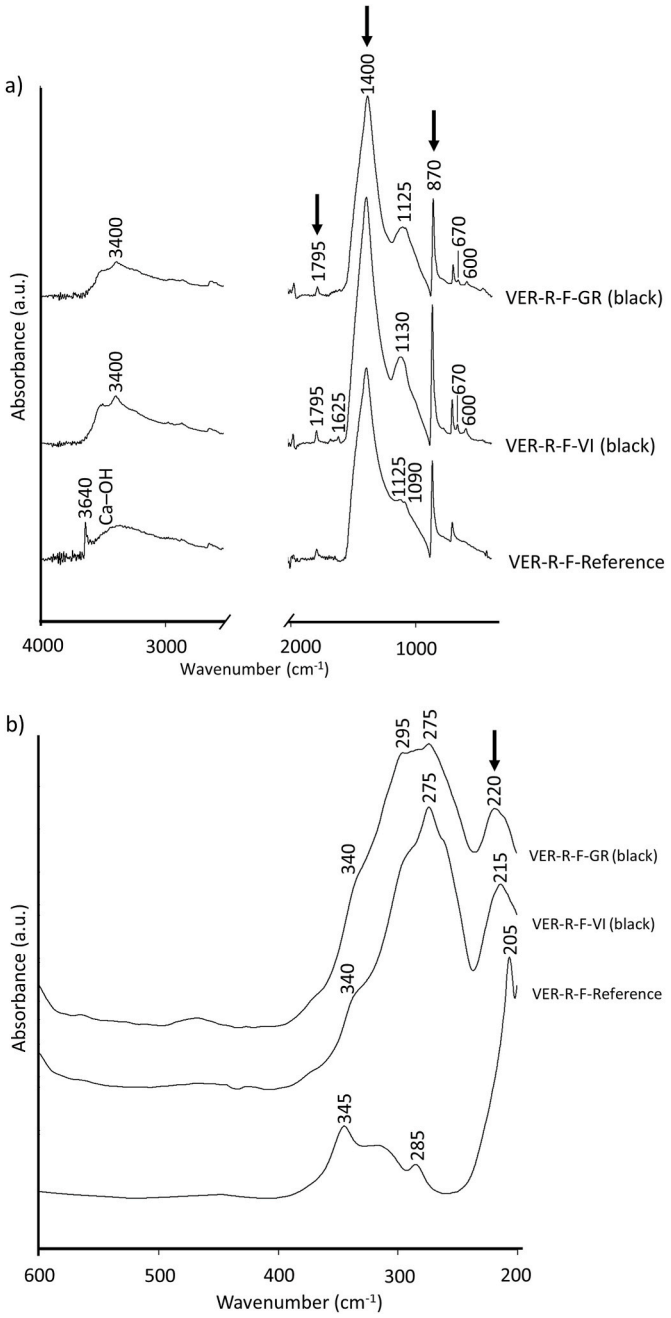


Fig. 6. ATR-FTIR spectra for VER-R-F: reference mock-ups and mock-ups exposed in Vigo (VI) and Granada (GR). a) Spectra in the mid-IR (4000-600 cm^{-1}) and b) in the far-IR (600-200 cm^{-1}) regions. Black arrows indicate the presence of characteristic calcium carbonate bands.

present in all the mock-ups, albeit as a single peak and at higher wavenumbers (≈1080 cm^{-1}) in UL-B-SB, MAR-R-SB and CHR-G-SB.

FTIR was also applied to the sulphide-based fresco paint mock-ups to study possible chemical changes that could explain the darkening of the surface. However, the spectra for the CIN-R-F and VER-R-F mock-ups did not show major changes when compared with those for the reference paints. Regardless of the colorimetric alteration (grey or black), the exposure site (VI or GR) or the pigment (CIN-R and VER-R), four new bands emerged in the mid-IR region (4000–600 cm^{-1}) after outdoor exposure (Fig. 6a). Small bands appeared at 3395 cm^{-1} (OH stretching), and at 1625, 670 and 602 cm^{-1} (SO_4^{2-} bending modes) [36,40]. In addition, the appearance of the two small bands present in the reference paint mock-ups at 1127 and 1090 cm^{-1} (Si–O asymmetric stretching [36]) changed, merging into a single, more intense band at ≈1130 cm^{-1} (S–O asymmetric stretching [36,40] after exposure. This newly-formed band at ≈1130 cm^{-1} related to the presence of gypsum [36,40] was slightly more intense in the samples from Vigo (*Csb*-type climate). As for the far-IR region (600–200 cm^{-1}), there was a change in the appearance of the strong bands at 345 and 285 cm^{-1} assigned to Hg–S tension of cinnabar/vermilion [41], present in the reference paint mock-ups (Fig. 6b), indicating changes in the molecular composition of the pigment. For both CIN-R-F and VER-R-F, a broad band emerged between 300 and 250 cm^{-1}, assigned to carbonates (marked with a black arrow in Fig. 6b). After exposure, the band at 345 cm^{-1} (Hg–S) was still present as a shoulder at ≈340 cm^{-1} while the peak at 205 cm^{-1} had disappeared. In addition, a new band could be seen at around 220 cm^{-1} assigned to CO_3^{2-} stretching (marked with a black arrow in Fig. 6b) and a broad band

between 300 and 250 cm^{-1} assigned to carbonates [42].

3.5. Raman spectroscopy (RS)

Raman was applied exclusively to the CIN-R and VER-R fresco paint mock-ups in a bid to observe the changes between the unaltered red paint and the grey, brown or black areas formed after outdoor exposure. Cinnabar and vermilion are known to have three Raman active optical-phonon frequency modes [43–45] at 250 cm^{-1} (bending vibration), and at 280 and 340 cm^{-1} (stretching vibration). Additional peaks at 100 cm^{-1} assigned to the lattice modes of cinnabar [43–45] and at 1083 cm^{-1}, CO_3 stretching assigned to calcite [46], were also present. All these Raman peaks were observed before and after exposure in all the sulphide-based fresco paints, regardless of the pigment, the colorimetric alteration (grey, brown or black) or the exposure site (VI or GR). According to Ref. [43], it is important to consider the 250–280 cm^{-1} range in the Raman spectra when studying the vibrational characteristics of reddish cinnabar and its possible transformation to blackish meta-cinnabar. As seen in Fig. 7, a very slight shift from 250 to 248 cm^{-1} occurred in CIN-R-F-GR (black and brown areas). However, no shifts were observed around 280 cm^{-1}. The same was observed in the Raman spectra for VER-R-F.

3.6. Polarized-Light Microscopy (PLM) and scanning electron microscopy with energy-dispersive X-ray spectroscopy (SEM-EDS)

When comparing the VI- and GR-exposed paints by the study of the cross-sections with Polarized-Light Microscopy (PLM), a whitish layer (also identified with the naked eye) could be observed on the surface of most of the paint mock-ups, regardless of the exposure site (VI or GR), the pigment used or the painting technique (F or SB). When studied with SEM-EDS, the presence of different nanometre-sized, rhombohedral calcium-rich particles was observed (Fig. 8a). This layer was thicker and more widespread in the Vigo samples (Fig. 8b and c) (around 15 μm as opposed to 8 μm in the Granada mock-ups). However, these Ca-rich deposits did not always cover the entire surface. Occasionally, smaller more scattered deposits were also unevenly distributed across the surface (as marked with a white arrow in Fig. 8d for the MAR-R-SB-VI sample). In the SB paint layers, these deposits were not only observed on the surface, but also under the paint layer, within the xerogel matrix itself, and filling the fissures (marked with white arrows in Fig. 8e). The precipitation of calcite could be due to the carbonation of $Ca(OH)_2$ that had not yet reacted. However, portlandite ($Ca(OH)_2$) was not identified by XRD in any of the samples. This suggests that the precipitation of calcite probably happened as follows: in the presence of atmospheric humidity and water (H_2O), calcium (Ca^{2+}) and carbonate ions (CO_3^{2-}) in the mortar substrate rose out of the mortar to the surface, where they reacted with atmospheric CO_2 and precipitated in the form of calcium carbonate ($CaCO_3$).

Various different situations were observed in the two exposure sites. In the specific case of GR-exposed paintings, with a *Dsa*-type climate, particles of different morphology (Fig. 9a) were observed on the surface of F and SB mock-ups alike. These particles were composed of calcium-Ca, silicon-Si, potassium-K, aluminium-Al, magnesium-Mg, iron-Fe, phosphor-P, barium-Ba, sulphur-S and titanium-Ti. In addition, deposits of irregular thickness (ranging between 2 and 40 μm) were observed in the cross-sections. These were composed of different small particles with the same chemical composition by EDS as the other particles (Fig. 9b and c). For their part, in the Vigo paint mock-ups (*Csb*-type climate), regardless of the painting technique or pigment used, individual particles rich in sodium-Na and chlorine-Cl (Fig. 9d and EDS spectra) were occasionally identified (with K, Mg and S as minor elements), as well as some phosphorus and potassium-rich particles (Fig. 9e and EDS spectra).

S- and Ca-rich particles were also observed sporadically on the surface of all the paint mock-ups, regardless of the painting technique, pigment used or exposure site. These particles displayed acicular (Fig. 10a, marked with a red triangle) and/or prismatic morphology (Fig. 10b, marked with a red triangle) and had a widespread presence in the CIN-R-F and VER-R-F mock-ups. Acicular-radiating crystals grouped in 'rosettes' of up to 100 μm wide were exclusively observed in the samples subject to *Csb*-type climate exposure in Vigo (Fig. 10c and EDS spectra). When comparing the SEM micrographs for CIN-R-SB or VER-R-SB, before and after exposure, it was observed that the xerogel surrounding the pigment particles showed fewer pigment particles, an increase in fissures and increased loss of silica xerogel (as marked with red arrows in Fig. 10d and e). Microtextural changes and fractures in the cinnabar particles were also observed (marked with a red triangle in Fig. 10f). These characteristics were observed in all the sulphide SB-paints regardless of the environmental conditions to which they were exposed (*Csb*- and *Dsa*-type climate).

The impurities present in the pigments were also influential, especially in LA-B, CIN-R, VER-R, and GE-G, regardless of the painting

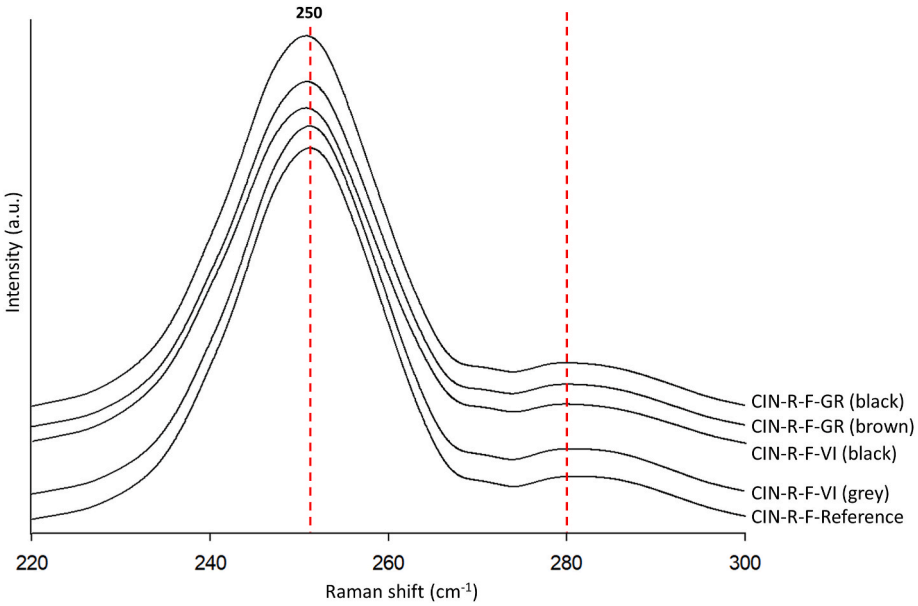


Fig. 7. Raman spectra in the region between 220 and 300 cm^{-1} for CIN-R-F paint mock-ups before and after exposure.

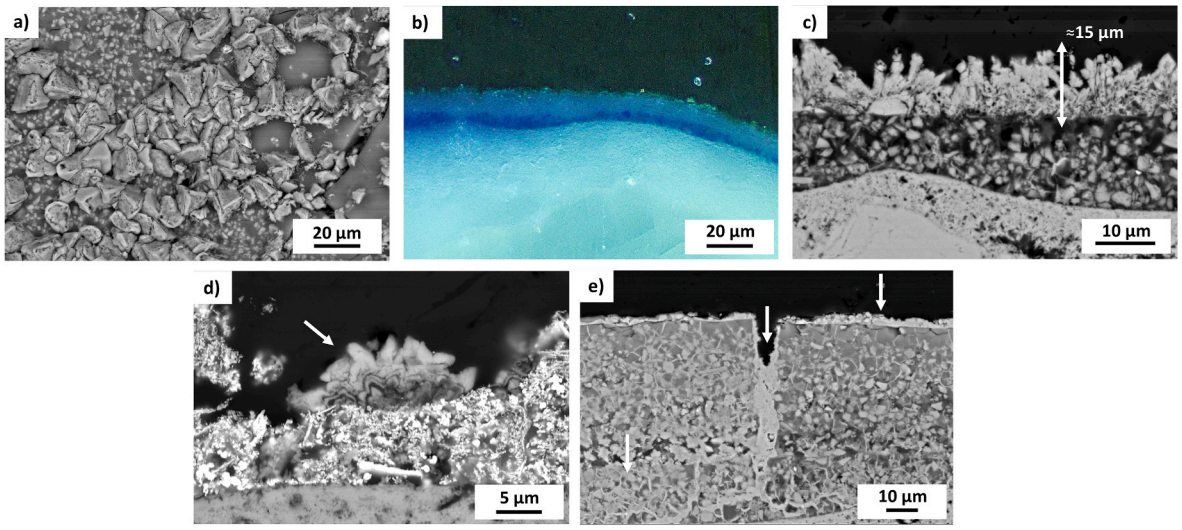


Fig. 8. a) SEM micrograph of UL-B-SB-VI; b) PLM micrograph of UL-B-SB-VI cross-section; c) SEM micrograph of UL-B-SB-VI; d) SEM micrograph of MAR-R-SB-VI cross-section; e) SEM micrograph of UL-B-SB-VI cross-section.

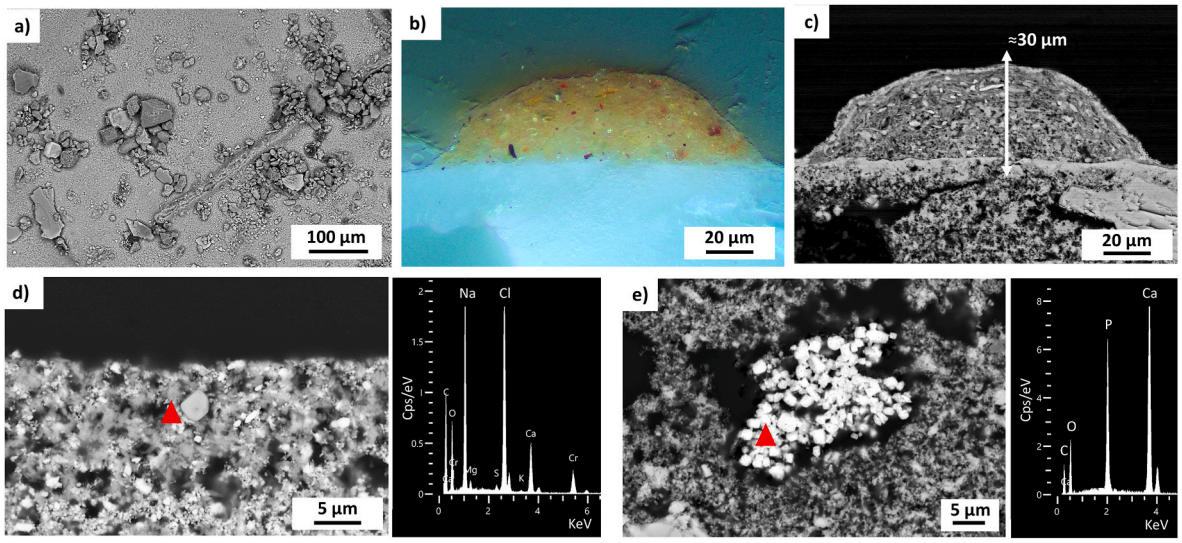


Fig. 9. a) SEM micrograph of FR-SB-GR; b) PLM micrograph and c) SEM micrograph of a brown deposit on FR-SB-GR cross-section; d) SEM micrograph of CHR-G-F-V cross-section with EDS spectra for the area marked with a red triangle; and e) SEM micrograph of FR-F-VI cross-section with EDS spectra for the area marked with a red triangle.

technique (F or SB) or exposure site (VI or GR). Under PLM, black particles were observed in the LA-B paint mock-ups (Fig. 11a). According to SEM-EDS, these were composed of S/Fe or Fe (Fig. 11b and c). In earlier research, [13] found unaltered pyrite (FeS_2) and iron oxide particles in these samples, which could be similar to those seen in Fig. 11b and c. Fissures were observed on the surface of these S/Fe-rich particles and were more pronounced on the edges (marked with red arrows in Fig. 11b and c). As for the sulphide-based paints, in PLM studies of the cross-sections, different blackish particles were detected, as seen in Fig. 11d, f and 11h. When studied by SEM-EDS, different chemical compositions were detected: i) S and zinc-Zn- (Fig. 11d and e and EDS spectra); and ii) S and antimony-Sb- (Fig. 11f and g and EDS spectra). By contrast, other particles with different colours (red and black) under PLM (marked with a square in Fig. 11h) turned out to have the same chemical composition (S, Hg) and textural appearance when studied by SEM-EDS (Fig. 11i). Finally, the SEM study of the GE-G-SB paint mock-ups showed poor cohesion between the nano-silica binder and the different pigment particles, especially in the Vigo samples (*Csb*-type climate). The apparent bond between the pigment particles and the xerogel matrix observed in the control mock-ups was not as strong as it seemed, as after exposure most of the pigment particles (rich in Si, Al, Ca and K) were no longer surrounded by the xerogel matrix (marked with red arrows in Fig. 11j) and there was a lack of adhesion between the SB paint layer and the mortar (marked with white arrows in Fig. 11j and k). Some of the particles were cracked and fractured (marked with a red arrow in Fig. 11k). Finally, even though there was no evidence of impurities in MAR-R, PLM observations of cross-sections of the samples painted with MAR-R-SB highlighted various blackish areas (Fig. 11l), something that was more pronounced in the GR samples. When these blackish areas were studied by SEM-EDS (Fig. 11m), they showed higher contrast. For their part, the X-ray maps for Fe and O revealed a higher presence of both elements. When the area was observed at higher magnifications, polyhedral particles could be seen (marked with white arrows in Fig. 11n).

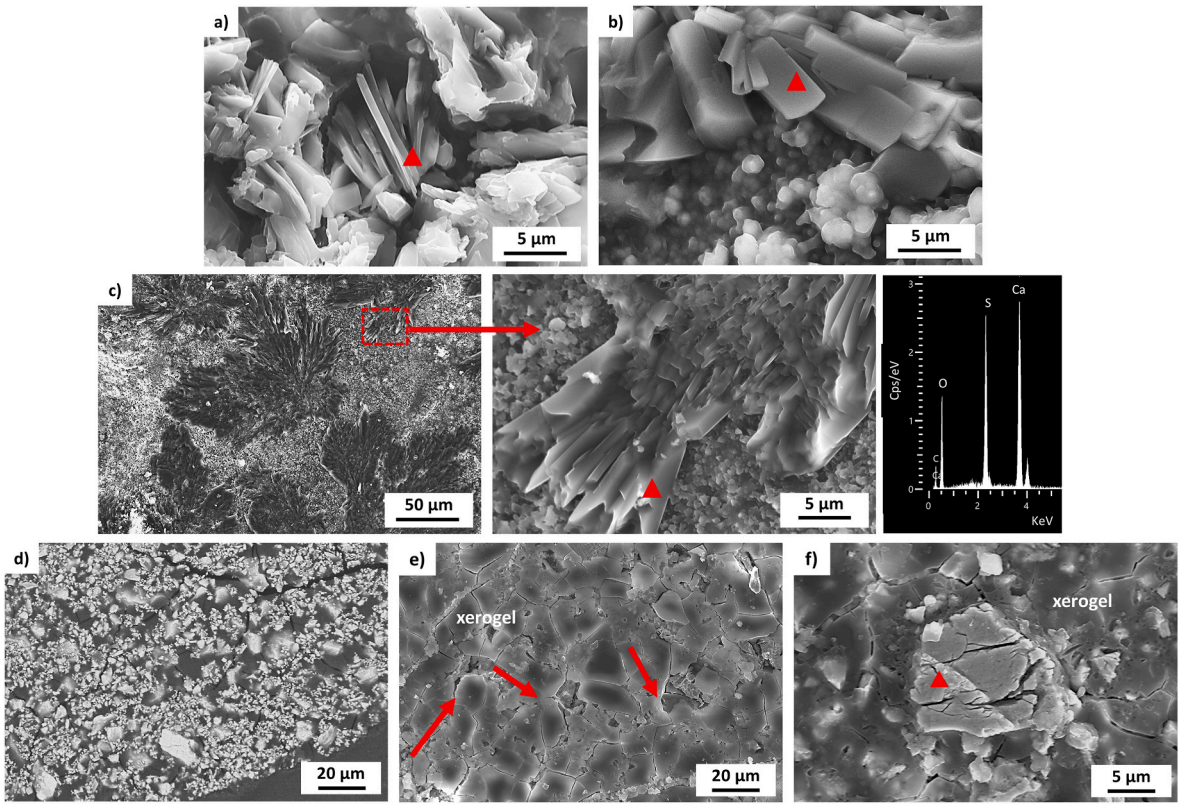


Fig. 10. SEM micrograph of calcium and sulphur-rich particles in a) LA-B-SB-VI; b) EG-B-F-VI; c) CIN-R-F-VI and EDS spectra for the area marked with a red triangle; d) CIN-R-SB micrograph before exposure and e-f) after exposure in Vigo (VI).

4. Discussion

The use of an aqueous dispersion of nano-sized silica as a binder for outdoor exposed wall paintings must be seen as a novel approach for several reasons. Firstly, due to the inadequacy of conventional inpainting techniques, justified by the extensive literature regarding their behaviour under different environmental agents in e.g. water-based [47–49] or varnish-based [50–54] procedures. Secondly, due to the lack of studies addressing the durability of non-conventional techniques e.g. mineral painting. In this regard, fewer studies have evaluated Na- or K-silicates, which have shown disadvantages though such as crack formation and insufficient water resistance [55–57]. Lastly, whilst the use of an aqueous dispersion of nano-sized silica has been widely evaluated as a consolidant [18–22], this is the first time that it has been evaluated as binder for chromatic reintegrations. Based on the results, the influence of the environment and of the chemical nature of the pigments were however highly influential and are discussed below.

4.1. Influence of the Csb- and Dsa-climatic conditions

In general terms, regardless of the painting technique and taking into account the total colour variation, the blue silicate- (EG-B, LA-B and UL-B) and oxide-based (MAR-R and CHR-G) paints remained unaltered at both sites with their respective environmental conditions. By contrast, the sulphide-based (F and SB) and green earth-based (only in SB) paints underwent major ΔE^*_{ab} variations which were initially more evident in the samples from Vigo, with a *Csb*-type climate. Nevertheless, by the end of the natural ageing test, ΔE^*_{ab} was similar at both sites. The only exception was LA-B-F-VI, which underwent major changes after exposure to *Csb*-climatic conditions. The ATR-FTIR, µXRD and SEM-EDS results indicate the formation of a calcium carbonate-based layer, not only on the surface, but also within the silica xerogel itself. The geographical location of Vigo (NW Spain) and its marine environment, with high relative humidity (an average of 76.9 % as opposed to 53.5 % in Granada) and high rainfall (128.6 L/m^2 as opposed to 28.3 L/m^2 in Granada) seem to have triggered the formation of a thicker, more widespread Ca-rich layer. Moreover, the rain in northern Spain is slightly more acidic (pH around 4.8 [58]) and is therefore likely to favour the dissolution of $CaCO_3$ and its subsequent reprecipitation. As for the formation of gypsum (also confirmed by ATR-FTIR, µXRD and SEM-EDS), when sulphur and Ca^{2+} are present in the water, an oxidation process takes place and sulphates can appear [59]. In Vigo, sulphur is likely to come from the sea (spray, mist or rain [60]) and/or from industrial or traffic pollution (SO_2 levels of 2.51 µg/m^3), whilst in Granada it is probably due to the high SO_2 values (8.58 µg/m^3). Furthermore, the Vigo mock-ups showed sporadic halite -NaCl-salts as a consequence of marine aerosol [61]. Fig. 9e also suggests the deposit of possibly apatite or hydroxyapatite ($Ca_5(PO_4)_3(F,Cl,OH)$) particles. These may originate from the phosphorus present in the rainwater in NW Spain [58] which, in the presence of high pH, can give rise to the formation of calcium phosphate phases [62,63].

The deposition of particulate matter was only observed in Granada (SE Spain), due to its proximity to the Sahara Desert in Africa. Its elemental composition by EDS coincides with that of various mineral phases identified in previous studies [64–66]: mainly aluminium phyllosilicates (e.g. kaolinite-$Al_2Si_2O_5(OH)_4$), tectosilicates (quartz-SiO_2), carbonates (dolomite-$CaMg(CO_3)_2$ and calcite-$CaCO_3$), barite ($BaSO_4$), iron oxy-hydroxides and organic matter.

4.2. Influence of the chemical composition of the pigment

Considering the chemical nature of the pigments as silicates, oxides and sulphides is determining when assessing the overall compatibility and durability of the chromatic reintegration. The best performing pigments in the SB paint mock-ups were the silicate- (except for GE-G) and oxide-based (MAR-R and CHR-G) pigments, which showed the

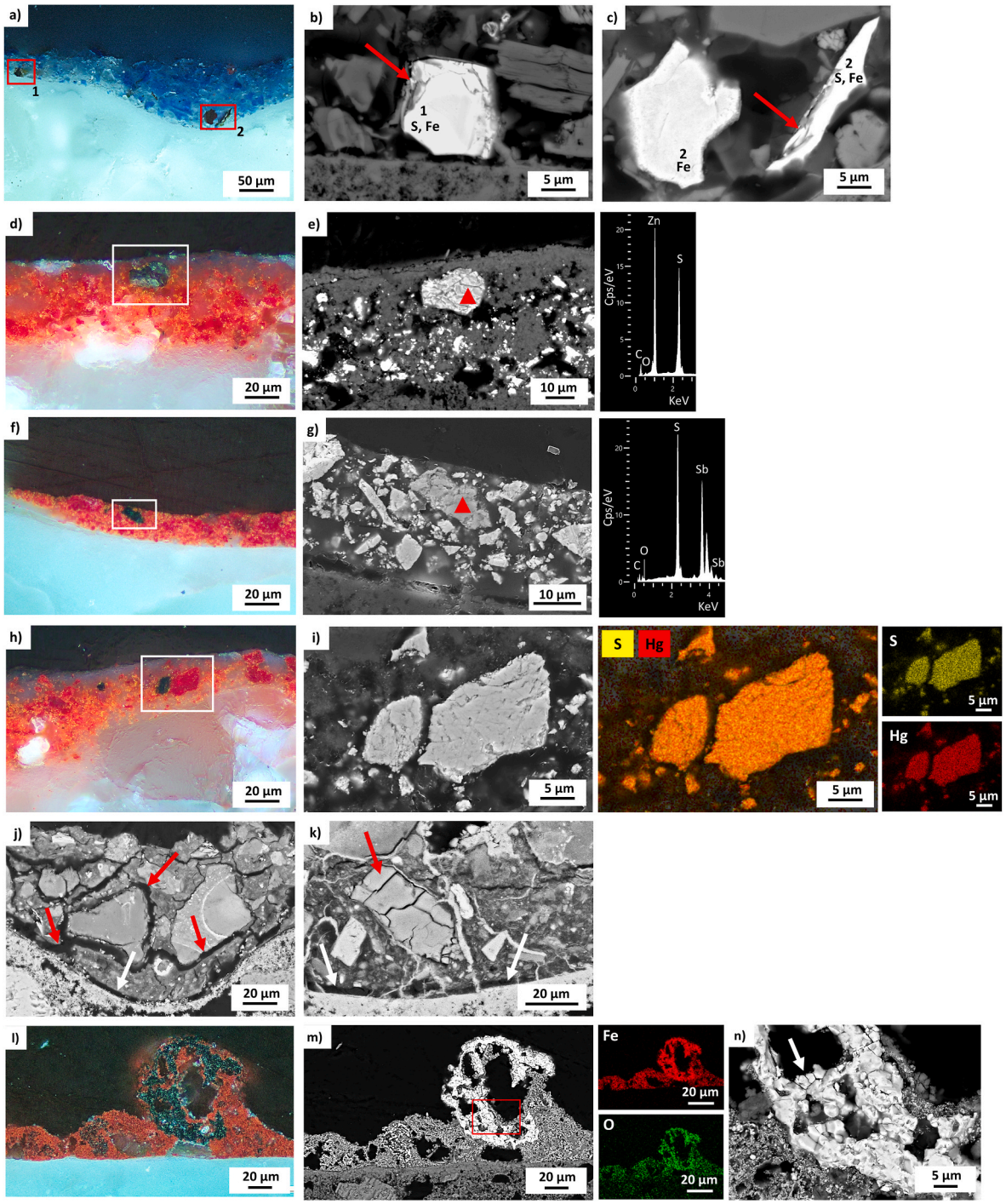


Fig. 11. a) PLM and SEM micrographs of cross-sections for: a-c) LA-B-SB-VI; d-e) CIN-R-F-GR; f-g) CIN-R-SB-GR; h-i) CIN-R-F-GR with X-ray maps; j-k) GE-G-SB-VI; and l-n) MAR-R-SB-GR with X-ray maps.

lowest levels of chromatic change and unaltered SB paint layers. The fissures that inevitably form on the surface of the xerogel (ass seen in Ref. [13]) were still present after exposure, with the same extent and thickness as before. This xerogel bonded very well with these pigments, creating a pictorial film with good adhesion to the lime-based mortar and no micro-textural changes after exposure. The higher chemical affinity of the aqueous dispersion of nano-sized silica with the blue-silicate pigments (EG-B, LA-B and UL-B) was due to the presence of siloxane groups (Si–O–Si) in the pigments, which are likely to form bonds with the xerogel's own siloxane groups. The affinity with oxide-based pigments, by contrast, could be related to the interaction of the oxides with water or moisture, which have led to the formation of hydroxyl groups, creating bonds with the silanol groups of the binder. This affinity was confirmed above all by the increased intensity of the FTIR bands assigned to the SiO_2 groups and the formation of silica gel, suggesting that silica formation was not hindered by the environmental conditions at either site, and in fact was enhanced by them.

The presence of impurities has also been seen as an issue to be considered to correctly assess the behaviour of the chromatic reintegration in the long-term. Future research should focus on this topic. Even though in LA-B paints pyrite and iron oxides underwent oxidation, and therefore blackening, these had no impact on ΔE^*_{ab} values as they

occurred sporadically and not at surface level. Even so, the oxidation of pyrite can generate acidic microenvironments and lead to the formation of gypsum due to the reaction with calcium [67]. This could be related to the higher ΔE^*_{ab} values observed in the LA-B-F mock-up in Vigo, where environmental conditions (higher moisture and higher acidic rains) could have triggered larger gypsum deposits. Lastly, even though MAR-R was one of the best-performing pigments, in that it showed the least ΔE^*_{ab}, Fig. 11l–n suggests that it did undergo some kind of transformation. It is possible that hexagonal α-Fe_2O_3 (red hematite) undergoes a reduction process and is transformed into octahedral Fe_3O_4 (black magnetite), as was found to have happened in alkaline environments [68] such as those created by the lime-based mortar.

The SB paint layers with GE-G, CIN-R and VER-R had practically disappeared after exposure. Although GE-G is a silicate like EG-B, LA-B and UL-B (which have shown stability during the one-year exposure), the presence of swelling clays such as montmorillonite, present as an impurity, could have influenced the behaviour of the paint layer and the bonding affinity between the binder (NE) and the pigment particles. Even though in the paint industry clay minerals may be added to the paint to improve its adhesion, large amounts of expandable clays can increase the risk of swelling [69,70]. Montmorillonite experiences osmotic swelling [71], which under variable moisture conditions can cause it to shrink or expand, so promoting paint loss. Furthermore, SEM-EDS also suggests that the natural origin of GE-G (i.e. varied chemical composition and presence of impurities) may also be a factor in the low affinity between the pigments and the xerogel, something that should be evaluated in future research. The markedly humid climate of Vigo must surely have influenced the lower affinity between GE-G and the NE binder.

As regards CIN-R and VER-R, their chemical composition based on S and Hg must have influenced their behaviour, by preventing the formation of –OH, Si–OH or Si–O bonds with the silica gel. In addition to the lack of bonding between the sulphide-based pigments and NE, another determining factor was the presence of impurities (which were not detected in the preliminary characterization of the pigments carried out by Ref. [13], probably because they were below the XRD detection threshold). The black particles observed in CIN-R-F and VER-R-F could be related to the minerals sphalerite (ZnS) and stibnite (Sb_2S_3) respectively, which are commonly associated with cinnabar ores [72,73]. As for the major colour variations i.e. the blackening that took place on the surface of the CIN-R and VER-R F paints, it has been widely reported in the literature [74,75] that these could be due to the transformation of hexagonal α–HgS (red cinnabar) to cubic β–HgS (black metacinnabar), even though the latter has not been identified in our samples. This aspect must be investigated further with higher-resolution techniques, such as transmission electron microscopy [76].

5. Conclusions

The aim of this study was to evaluate the durability of an aqueous colloidal solution of nano-sized silica particles as a binder for chromatic reintegrations on partially or completely exposed wall paintings. The environmental conditions to which the mock-ups were exposed in Granada and Vigo were seen as determining factors in the durability of the paints, and the prevailing *Csb*-climate of NW Spain was found to be more influential. Indeed, the higher moisture, the higher levels of slightly acidic rainfall, together with the influence of the Atlantic Sea, led to the deposit of a thicker, more extensive layer of calcium carbonate, and the formation of chlorides and phosphates of marine origin. As for the *Dsa*-type climate in Granada, although the calcium carbonate layer was thinner, the proximity of SE Spain to Africa favoured the deposition of particulate matter. As for the influence of the pigments on the nano-silica-based chromatic reintegrations, the oxide-based (mars red and chromium green) and silicate-based (Egyptian blue, lapis lazuli and blue ultramarine) paints remained unaltered due to their higher chemical affinity with the binder, which promoted the formation of bonds with the hydroxyl, silanol and/or siloxane groups of the SiO_2 binder. Green earth showed low affinity, mainly due to the presence of phyllosilicates that swelled up and other impurities. As for the sulphide-based pigments (cinnabar and vermilion), their chemical composition was incompatible with the nano-silica binder. Ultimately, this study has highlighted the need to evaluate in depth the influence that impurities can have on the durability of chromatic reintegrations or in other restoration works that involve the use of pigments.

Although this research confirms the validity of the procedure developed in previous research for inpainting the lacunae in wall paintings partially or completely exposed to outdoor environmental conditions, it is important to bear in mind that this is an experimental study based on mock-up paints. A historical wall painting is affected not only by the layers of mortar that lie beneath it, but also by many other factors, such as the material from which the wall is made (e.g. brick or stone), its orientation (north, south, etc), the traffic etc., all of which will influence the overall behaviour of the paints. Therefore, in the future, the long-term durability of these chromatic reintegrations should be evaluated in real outdoor exposed artworks and for a longer period, to further validate this inpainting technique.

In short, professionals should consider the chemical nature of the pigments, since only the silicates and oxides used in this study have shown stability over time. Exposure conditions are also influential as high humidity induced by coastal environment produced greater deterioration processes. Finally, for this inpainting technique to be considered suitable in line with the ethics of the restoration profession and the stipulations of the different international heritage organisations (UNESCO, ICOMOS, etc.), it must be reversible, which means that in future research, reversibility tests must be carried out to ensure that this requirement is also met.

CRediT authorship contribution statement

Daniel Jiménez-Desmond: Writing – original draft, Visualization, Software, Resources, Methodology, Investigation, Formal analysis, Data curation, Conceptualization. **José Santiago Pozo-Antonio:** Writing – review & editing, Validation, Supervision, Software, Resources, Project administration, Methodology, Funding acquisition, Conceptualization. **Anna Arizzi:** Writing – review & editing, Validation, Supervision, Software, Resources, Project administration, Methodology, Funding acquisition, Conceptualization.

Declaration of competing interest

The authors declare that they have no known competing financial interests or personal relationships that could be construed to have influenced the work reported in this paper in any way.

Acknowledgments

This study was funded by the Xunta de Galicia ED431F 2022/07 research project. Daniel Jiménez-Desmond was supported by the ED481A-2023/086 predoctoral contract through “Programa de axudas á etapa predoutoral da Xunta de Galicia” cofinanced by the European Union within the framework of the FSE+ Galicia 2021–2027 programme. José Santiago Pozo-Antonio was supported by the RYC2020-028902-I project funded by MICIU/AEI/10.13039/501100011033 and, by “ESF Investing in your future”. Anna Arizzi was funded by the State Research Agency (SRA) and the Ministry of Science and Innovation under Research Project PID2020-119838RA-I00. within the Junta de Andalucía Research Group RNM179. For more information, see https://laseringph.webs.uvigo.es/.

Appendix A. Supplementary data

Supplementary data to this article can be found online at https://doi.

org/10.1016/j.dyepig.2025.112651.

Data availability

Data will be made available on request.

References

[1] Gallego Roca J. Criterios y metodologías para la conservación y restauración de los revestimientos y el color en la arquitectura. Loggia, Arquitectura & Restauración 1997;2:68–72.
[2] Cardenyes JM. Pintura mural al fresco: estrategias de los pintores. Lleida: Universitat de Lleida; 2014.
[3] Matteini M, Moles A. La química en la restauración: los materiales del arte pictórico, Editorial Nerea. Guipúzcua. 2001.
[4] Mora L, Mora P, Philippot P. La conservazione delle pitture murali. Bologna: Editrice Compositori; 1999.
[5] Venegas García C, Barrainkua Legid A. La conservación de pintura mural. Síntesis. 2021. Madrid.
[6] Giannini C. Dizionario del Restauro. In: Techniche diagnostica, convervazione, nardini editore; 2010. Perugia, Italy.
[7] Mercado Hervás MS. Técnicas y procedimientos de reintegración cromática. Cuadernos de Restauración 2009;7:5–12.
[8] Jiménez-Desmond D, Pozo-Antonio JS, Arizzi A. Present and future of chromatic reintegrations of wall paintings. J Cult Herit 2024;67:237–47. https://doi.org/10.1016/j.culher.2024.03.010.
[9] Baglioni P, Giorgi R. Inorganic nanomaterials for the consolidation of wall paintings and stones. In: Baglioni P, Chelazzi D, editors. Nanoscience for the conservation of works of art. RSC Publishing; 2013. p. 345–71.
[10] Napoleone L. Integrazione pittorica. Acqua sporca, sottotono, tinta neutra, rigatino. Progetto Colore 2008;2:21–2.
[11] Brandi C. Teoria del restauro. Firenze: Nardini Editore; 2011.
[12] Sánchez Pons M, Sanesi Bigagli D. Los silicatos como aglutinantes pictóricos de pinturas murales en los siglos XX y XXI: caracterización de las principales tipologías. Ge-Conservación 2021;20:318–36.
[13] D. Jiménez-Desmond, J.S. Pozo-Antonio, A. Arizzi, Assessment of the physical-chemical compatibility of a nano-size silica dispersion as binder for chromatic reintegration in fresco wall paintings, Journal of Cultural Heritage. UNDER REVISION (n.d.).
[14] Zornoza-Indart A, Lopez-Arce P. Silica nanoparticles (SiO2): influence of relative humidity in stone consolidation. J Cult Herit 2016;18:258–70. https://doi.org/10.1016/j.culher.2015.06.002.
[15] Zhuravlev LT. The surface chemistry of amorphous silica. Zhuravlev model. Colloids Surf A Physicochem Eng Asp 2000;173. www.elsevier.nl/locate/colsurfa. [Accessed 19 March 2024].
[16] De Ferri L, Lottici PP, Lorenzi A, Montenero A, Salvioli-Mariani E. Study of silica nanoparticles - polysiloxane hydrophobic treatments for stone-based monument protection. J Cult Herit 2011;12:356–63. https://doi.org/10.1016/j.culher.2011.02.006.
[17] Di Crescenzo MM, Zendri E, Sánchez-Pons M, Fuster-López L. Inpainting modern and contemporary murals: study of the stability of some retouching materials. In: Sánchez Pons M, Shank W, Fuster López L, editors. Conservation issues in modern and contemporary murals. Newcastle: Cambridge Scholars Publishing; 2012. p. 323–38.
[18] Pozo-Antonio JS, Otero J, Alonso P, Mas i Barberà X. Nanolime- and nanosilica-based consolidants applied on heated granite and limestone: effectiveness and durability. Constr Build Mater 2019;201:852–70. https://doi.org/10.1016/J.CONBUILDMAT.2018.12.213.
[19] Erfan AM, Hassan HE, Hatab KM, El-Sayed TA. The flexural behavior of nano concrete and high strength concrete using GFRP. Constr Build Mater 2020;247. https://doi.org/10.1016/j.conbuildmat.2020.118664.
[20] Ripoll A, Rojo A, de Argandoña VGR. Evaluation of nanoparticulate consolidants applied to Novelda Stone (Spain). Mater Construcción 2022;72. https://doi.org/10.3989/mc.2022.11621.
[21] Costanzo A, Ebolese D, Ruffolo SA, Falcone S, la Piana C, La Russa MF, Musacchio M, Buongiorno MF. Detection of the TiO2 concentration in the protective coatings for the cultural heritage by means of hyperspectral data. Sustainability 2021;13. https://doi.org/10.3390/su13010092.
[22] Iucolano F, Colella A, Liguori B, Calcaterra D. Suitability of silica nanoparticles for tuff consolidation. Constr Build Mater 2019;202:73–81. https://doi.org/10.1016/j.conbuildmat.2019.01.002.
[23] Coccato A, Moens L, Vandenabeele P. On the stability of mediaeval inorganic pigments: a literature review of the effect of climate, material selection, biological activity, analysis and conservation treatments. Herit Sci 2017;5. https://doi.org/10.1186/s40494-017-0125-6.
[24] Data Sheet, Nano ESTEL. Consolidant and fixativ product for natural stone, brick, terracotta, mortars and plasters, C.T.S. S.R.L. (n.d.) 1–3. https://www.ctseurope.com/gb/251-nano-estel (accessed June 19, 2023).
[25] CIE S014-4/E:2007, Colorimetry-part 4: CIE 1976 L* a* b* colour space. International Standard; 2007.
[26] CIE Publication 15-2. Colorimetry CIE central bureau. 1986.
[27] UNE-EN ISO 2813, Pinturas y barnices. Determinación del índice de brillo especular a 20°, 60° y 85°. Madrid: AENOR; 2015.
[28] Mokrzycki W, Tatol M. Color difference Delta E-A survey Colour difference ΔE-A survey, Machine. Graphics and Vision 2011;20:383–411. https://www.researchgate.net/publication/236023905.
[29] Bentabol M, Ruiz Cruz MD, Huertas FJ, Linares J. Hydrothermal transformation of kaolinite to illite at 200 and 300 ° C. Clay Miner 2003;38:161–72. https://doi.org/10.1180/0009855033820086.
[30] Hsiao YH, Shen YH, Ray DT. Synthesis of ultramarine from reservoir silts. Minerals 2017;7. https://doi.org/10.3390/min7050069.
[31] Echeverrie M, Giraldo LF, López BL. Synthesis and functionalization of silica nanoparticles with spherical morphology. Scientia et Technica Año XIII 2007;36:169–73. http://www.redalyc.org/articulo.oa?id=84903632.
[32] Balas F, Rodríguez-Delgado M, Otero-Arean C, Conde F, Matesanz E, Esquivias L, Ramírez-Castellanos J, Gonzalez-Calbet J, Vallet-Regí M. Structural characterization of nanosized silica spheres. Solid State Sci 2007;9:351–6. https://doi.org/10.1016/j.solidstatesciences.2007.03.004.
[33] Rao KS, El-Hami K, Kodaki T, Matsushige K, Makino K. A novel method for synthesis of silica nanoparticles. J Colloid Interface Sci 2005;289:125–31. https://doi.org/10.1016/j.jcis.2005.02.019.
[34] Echeverri E M, Fernando Giraldo L, Lucy López B. Synthesis and functionalization of silica nanoparticles with spherical morphology. Scientia et Technica Año XIII 2007;36:169–73.
[35] Fernández-Carrasco L, Torrens-Martín D, Morales LM, Martínez-Ramírez S. Infrared spectroscopy in the analysis of building and construction materials. In: Theophanides T, editor. Infrared spectroscopy: materials science, engineering and technology. Rijeka, Croatia: InTech; 2012. p. 369–81.
[36] Derrick MR, Stulik D, Landry JM. Scientific tools for conservation. Infrared spectroscopy in conservation science. Los Angeles: The Getty Conservation Institute; 1999.
[37] Loy CW, Matori KA, Lim WF, Schmid S, Zainuddin N, Wahab ZA, Alassan ZN, Zaid MHM. Effects of calcination on the crystallography and nonbiogenic aragonite formation of ark clam shell under ambient condition. Adv Mater Sci Eng 2016;2016. https://doi.org/10.1155/2016/2914368.
[38] Horgines M, Chen JJ, Bouillon C. Overview about the use of Fourier transform infrared spectroscopy to study cementitious materials. In: WIT transactions on engineering sciences; 2013. p. 251–62. https://doi.org/10.2495/MC130151. WITPress.
[39] Coimbra MM, Martins I, Bruno SM, Vaz PD, Ribeiro-Claro PJA, Rudić S, Nolasco MM. Shedding light on cuprorivaite, the Egyptian blue pigment: joining neutrons and photons for a computational spectroscopy study. Cryst Growth Des 2023;23:4961–9. https://doi.org/10.1021/acs.cgd.3c00211.
[40] Hass M, Sutherland G. The infra-red spectrum and crystal structure of gypsum. Proc R Soc Lond A Math Phys Sci 1956;236:427–45. https://doi.org/10.1098/RSPA.1956.0146.
[41] Vahur S, Knuutinen U, Leito I. ATR-FT-IR spectroscopy in the region of 500-230 cm-1 for identification of inorganic red pigments. Spectrochim Acta Mol Biomol Spectrosc 2009;73:764–71. https://doi.org/10.1016/j.saa.2009.03.027.
[42] Campbell S, Poduska KM. Incorporating far-infrared data into carbonate mineral analyses. Minerals 2020;10. https://doi.org/10.3390/min10070628.
[43] Chiriu D, Pala M, Pisu FA, Cappellini G, Ricci PC, Carbonaro CM. Time through colors: a kinetic model of red vermilion darkening from Raman spectra. Dyes Pigments 2021;184. https://doi.org/10.1016/j.dyepig.2020.108866.
[44] Zallen R, Lucovsky G, Taylor W, Pinczuk A, Burstein E. Lattice vibrations in trigonal HgS. Phys Rev B 1970;1:4058. https://doi.org/10.1103/PhysRevB.1.4058.
[45] Nusimovici MA, Meskaoui A. Raman scattering by α-HgS (cinnabar). Phys Status Solidi 1973;58:121–5. https://doi.org/10.1002/PSSB.2220580112.
[46] Kim Y, Caumon MC, Barres O, Sall A, Cauzid J. Identification and composition of carbonate minerals of the calcite structure by Raman and infrared spectroscopies using portable devices. Spectrochim Acta Mol Biomol Spectrosc 2021;261:119980. https://doi.org/10.1016/J.SAA.2021.119980.
[47] Bonifazi G, Capobianco G, Pelosi C, Serranti S. Hyperspectral imaging as powerful technique for investigating the stability of painting samples. J Imaging 2019;5. https://doi.org/10.3390/jimaging5010008.
[48] Pelosi C, Capobianco G, Agresti G, Bonifazi G, Morresi F, Rossi S, Santamaria U, Serranti S. A methodological approach to study the stability of selected watercolours for painting reintegration, through reflectance spectrophotometry, Fourier transform infrared spectroscopy and hyperspectral imaging. Spectrochim Acta Mol Biomol Spectrosc 2018;198:92–106. https://doi.org/10.1016/j.saa.2018.03.008.
[49] Capasso FE, Giandomenico M, Muca S, Gaetani MC, Iafrate S, Bartolini M, Santamaria U, Calia A, Vasanelli E, Melica D. Retouching mural paintings in hypogeum: preliminary study and first results. In: RECH6 - 6th International Meeting on Retouching of Cultural Heritage, Universitat Politecnica de Valencia, Valencia; 2021. https://doi.org/10.4995/rech6.2021.13533.
[50] Jin Choi H, Ill Kang D. A study on the retouching materials for oil paintings: using restoration colors. Journal of Conservation Science 2022;38:558–75. https://doi.org/10.12654/JCS.2022.
[51] Sánchez Ortiz A, Sánchez Ledesma A, Micó Boró S. Assessment of colour differences in three contemporary materials for the chromatic reintegration of cultural property. Opt Pura Apl 2010;43:141–51. www.sedoptica.es.
[52] Poli T, Piccirillo A, Nervo M, Chiantore O. Interactions of natural resins and pigments in works of art. J Colloid Interface Sci 2017;503:1–9. https://doi.org/10.1016/j.jcis.2017.04.094.
[53] de la Rie ER, Lomax SQ, Palmer M, Glinsman LD, Maines CA. An investigation of the photochemical stability of urea-aldehyde resin retouching paints: removability

tests and colour spectroscopy. Stud Conserv 2000;45:51–9. https://doi.org/10.1179/sic.2000.45.supplement-1.51.
[54] Dietemann P, Higgitt C, Kälin M, Edelmann MJ, Knochenmuss R, Zenobi R. Aging and yellowing of triterpenoid resin varnishes - influence of aging conditions and resin composition. J Cult Herit 2009;10:30–40. https://doi.org/10.1016/j.culher.2008.04.007.
[55] Gridchin AM, Loganina VI, Mazhitov EB, Ryapukhin AN. Assessment of the durability of coatings based on sol silicate paint. In: Klyuev S, Lesovik V, Vatin N, editors. International scientific conference on innovations and technologies in construction; 2020. p. 227–32.
[56] Kartsonakis IA, Koumoulos EP, Balaskas AC, Pappas GS, Charitidis CA, Kordas GC. Hybrid organic-inorganic multilayer coatings including nanocontainers for corrosion protection of metal alloys. Corros Sci 2012;57:56–66. https://doi.org/10.1016/j.corsci.2011.12.034.
[57] Loganina V, Mazhitov Y, Fediuk R, Nikolai V, Timokhin R. Advanced sol-silicate paint. In: Anatolijs B, Nikolai V, Vitalii S, editors. EECE 2019, lecture notes in civil engineering. Springer; 2020. p. 67–79.
[58] Vázquez A, Costoya M, Peña RM, García S, Herrero C. A rainwater quality monitoring network: a preliminary study of the composition of rainwater in Galicia (NW Spain). Chemosphere 2003;51:375–86. https://doi.org/10.1016/S0045-6535(02)00805-6.
[59] Kontozova-Deutsch V, Cardell C, Urosevic M, Ruiz-Agudo E, Deutsch F, Van Grieken R. Characterization of indoor and outdoor atmospheric pollutants impacting architectural monuments: the case of San Jerónimo Monastery (Granada, Spain). Environ Earth Sci 2011;63:1433–45. https://doi.org/10.1007/s12665-010-0657-5.
[60] Rivas T, Pozo S, Paz M. Sulphur and oxygen isotope analysis to identify sources of sulphur in gypsum-rich black crusts developed on granites. Sci Total Environ 2014;482–483:137–47. https://doi.org/10.1016/j.scitotenv.2014.02.128.
[61] Morillas H, Maguregui M, Gallego-Cartagena E, Marcaida I, Carral N, Madariaga JM. The influence of marine environment on the conservation state of Built Heritage: an overview study. Sci Total Environ 2020;745:140899. https://doi.org/10.1016/J.SCITOTENV.2020.140899.
[62] Oliveira C, Georgieva P, Rocha F, Ferreira A, Feyo de Azevedo S. Dynamical model of brushite precipitation. J Cryst Growth 2007;305:201–10. https://doi.org/10.1016/j.jcrysgro.2007.04.016.
[63] Arifuzzaman SM, Rohani S. Experimental study of brushite precipitation. J Cryst Growth 2004;267:624–34. https://doi.org/10.1016/j.jcrysgro.2004.04.024.
[64] Kontozova-Deutsch V, Cardell C, Urosevic M, Ruiz-Agudo E, Deutsch F, Van Grieken R. Characterization of indoor and outdoor atmospheric pollutants impacting architectural monuments: the case of San Jerónimo Monastery (Granada, Spain). Environ Earth Sci 2011;63:1433–45. https://doi.org/10.1007/s12665-010-0657-5.
[65] Molinero-García A, Martín-García JM, Fernández-González MV, Delgado R. Provenance fingerprints of atmospheric dust collected at Granada city (Southern Iberian Peninsula). Evidence from quartz grains. Catena 2022;208. https://doi.org/10.1016/J.CATENA.2021.105738.
[66] Fernández-Caliani JC, Barba-Brioso C, González I, Galán E. Heavy metal pollution in soils around the abandoned mine sites of the iberian pyrite belt (Southwest Spain). Water Air Soil Pollut 2009;200:211–26. https://doi.org/10.1007/s11270-008-9905-7.
[67] Cockell CS, Pybus D, Olsson-Francis K, Kelly L, Petley D, Rosser N, Howard K, Mosselmans F. Molecular characterization and geological microenvironment of a microbial community inhabiting weathered receding shale cliffs. Environ Microbiol 2011;61:166–81. https://doi.org/10.1007/s00248-010-9730-6.
[68] feng Lu J, Tsai CJ. Hydrothermal phase transformation of hematite to magnetite. Nanoscale Res Lett 2014;9:1–8. https://doi.org/10.1186/1556-276X-9-230.
[69] Hradil D, Bezdička P, Hradilová J, Vašutová V. Microanalysis of clay-based pigments in paintings by XRD techniques. Microchem J 2016;125:10–20. https://doi.org/10.1016/J.MICROC.2015.10.032.
[70] Fanost A, Jaber M, de Viguerie L, Korb JP, Levitz PE, Michot LJ, Mériguet G, Rollet AL. Green earth pigments dispersions: water dynamics at the interfaces. J Colloid Interface Sci 2021;581:644–55. https://doi.org/10.1016/J.JCIS.2020.07.085.
[71] Paineau E, Bihannic I, Baravian C, Philippe AM, Davidson P, Levitz P, Funari SS, Rochas C, Michot LJ. Aqueous suspensions of natural swelling clay minerals. 1. structure and electrostatic interactions. Langmuir 2011;27:5562–73. https://doi.org/10.1021/la2001255.
[72] Loredo J, Luque Cabal C, Garcia Iglesias J. Conditions of formation of mercury deposits from the Cantabrian zone (Spain). Bull Mineral 1988;111:393–400. https://doi.org/10.3406/BULMI.1988.8060.
[73] Gettens RJ, Feller RL, Chase WT. Vermilion and cinnabar. In: Roy A, editor. Artists pigments. A handbook of their history and characteristics. London: Archetype Publications; 1993. p. 159–82.
[74] Gliozzo E. Pigments — mercury-based red (cinnabar-vermilion) and white (calomel) and their degradation products. Archaeol Anthropol Sci 2021. https://doi.org/10.1007/s12520-021-01402-4/Published.
[75] Elert K, Pérez Mendoza M, Cardell C. Direct evidence for metallic mercury causing photo-induced darkening of red cinnabar tempera paints. Commun Chem 2021;4. https://doi.org/10.1038/s42004-021-00610-2.
[76] Jeong HY, Sun K, Hayes KF. Microscopic and spectroscopic characterization of Hg (II) immobilization by mackinawite (FeS). Environ Sci Technol 2010;44:7476–83. https://doi.org/10.1021/es100808y.